**Title**
Polymer Nanocomposite Materials with High Dielectric Permittivity and Low Dielectric Loss Properties



**Author**
Toor, Anju

**Publication Date**
2017

Peer reviewed|Thesis/dissertation

**Polymer Nanocomposite Materials with High Dielectric Permittivity and Low Dielectric Loss Properties**

by

Anju Toor

A dissertation submitted in partial satisfaction of the
requirements for the degree of
Doctor of Philosophy

in

Engineering - Mechanical Engineering

in the

Graduate Division

of the

University of California, Berkeley

Committee in charge:

Professor Tarek Zohdi, Co-chair
Professor Albert P. Pisano, Co-chair
Professor Liwei Lin
Professor Ali Javey

Spring 2017

**Polymer Nanocomposite Materials with High Dielectric Permittivity and Low Dielectric Loss Properties**

## Abstract

Polymer Nanocomposite Materials with High Dielectric Permittivity and Low Dielectric Loss Properties

by

Anju Toor

Doctor of Philosophy in Engineering - Mechanical Engineering

University of California, Berkeley

Professor Tarek Zohdi, Co-chair

Professor Albert P. Pisano, Co-chair

Materials with high dielectric permittivity have drawn increasing interests in recent years for their important applications in capacitors, actuators, and high energy density pulsed-power. Particularly, polymer-based dielectrics are excellent candidates, owing to their properties such as high breakdown strength, low dielectric loss, flexibility and easy processing. To enhance the dielectric permittivity of polymer materials, typically, high dielectric constant filler materials are added to the polymer. Previously, ferroelectric and conductive fillers have been mainly used. However, such systems suffered from various limitations. For example, composites based on ferroelectric materials like barium titanate, exhibited high dielectric loss, and poor saturation voltages. Conductive fillers are used in the form of powder aggregates, and they may show 10-100 times enhancement in dielectric constant, however these nanoparticle aggregates cause the dielectric loss to be significant. Also, agglomerates limit the volume fraction of fillers in polymer and hence, the ability to achieve superior dielectric constants. Thus, the aggregation of nanoparticles is a significant challenge to their use to improve the dielectric permittivity.

We propose the use of ligand-coated metal nanoparticle fillers to enhance the dielectric properties of the host polymer while minimizing dielectric loss by preventing nanoparticle agglomeration. The focus is on obtaining uniform dispersion of nanoparticles with no agglomeration by utilizing appropriate ligands/surface functionalizations on the gold nanoparticle surface. Use of ligand coated metal nanoparticles will enhance the dielectric constant while minimizing dielectric loss, even with the particles closely packed in the polymer matrix. Novel combinations of materials, which use 5 nm diameter metal nanoparticles embedded inside high breakdown strength polymer materials are evaluated. High breakdown strength polymer materials are chosen to allow further exploration of these materials for energy storage applications.

In summary, two novel nanocomposite materials are designed and synthesized, one involving polyvinylidene fluoride (PVDF) as the host polymer for potential applications in

energy storage and the other with SU-8 for microelectronic applications. Scanning electron microscopy (SEM), transmission electron microscopy (TEM), energy dispersive X-ray spectroscopy and ultramicrotoming techniques were used for the material characterization of the nanocomposite materials. A homogeneous dispersion of gold nanoparticles with low particle agglomeration has been achieved. Fabricated nanoparticle polymer composite films showed the absence of voids and cracks. Also, no evidence of macro-phase separation of nanoparticles from the polymer phase was observed. This is important because nanoparticle agglomeration and phase separation from the polymer usually results in poor processability of films and a high defect density. Dielectric characterization of the nanocomposite materials showed enhancement in the dielectric constant over the base polymer values and low dielectric loss values were observed.

To my parents Satvir and Savitri.

# Contents

# List of Figures

# List of Tables

## Acknowledgments

I would like to express my deepest appreciation to my advisor Prof. Albert P. Pisano for his continued support and guidance. He provided me the freedom to follow my research interests. Thank you for providing the opportunity to pursue doctoral studies under your supervision. I would also like to express my sincere thanks to my committee members Prof. Tarek Zohdi, Prof. Liwei Lin and Prof. Ali Javey for their feedback and advice throughout the doctoral studies and during the dissertation writing.

I express my sincere gratitude to Dr. Jim Cheng who served as a mentor and provided invaluable guidance. I enjoyed my stimulating research discussions with him. I would also like to thank my labmates in the Pisano Research for Integrated Micromechanical and Electrical (PRIME) Systems Laboratory for their discerning feedback and support.

I am really thankful to my friend Animesh Garg for his support and valuable feedback. Finally, I would like to thank my parents for their never ending love and continuous support. Without their encouragement and support, I could not have make my dream of studying abroad come true.

# Chapter 1

# Introduction

To meet the needs of future power generation and distribution, improved and efficient energy storage devices are required. The market for electric energy storage is continuously emerging (Figure 1.1), mainly driven by applications based on electric mobility for example, electronics and plug in vehicles, including new applications such as stationery energy storage in power grids. This need of efficient energy storage drives the development of new materials and their implementation into devices remains a major challenge in the energy research. Batteries, capacitors, fuel cells, and solid-state film capacitors are the main electrical energy storage technologies for consumer markets. Performance of these energy storage mechanisms is usually evaluated in terms of two key parameters, one is energy density i.e. how long the stored energy can supply/last and the other is power density which implies how fast the energy can be released.

Current energy storage mechanisms such as batteries and fuel cells have high energy density but are not suitable for high power applications due to the slow reaction kinetics of the battery electrodes and the mass transport of the reactants. Supercapacitors can handle high power rates, but they have moderate energy storage capacities, and suffer from low operating voltages and high leakage currents. This prevents their usage in pulsed power applications. Furthermore, their power density is low. In contrast, capacitors based on solid-state dielectric films have high power density due their fast charge-discharge characteristics but their energy density is low. The energy density in solid-state capacitors depends on the dielectric permittivity and the breakdown strength of the dielectric materials that separate the oppositely charged electrodes. The aim of this thesis is to develop solid-state dielectric materials with enhanced dielectric properties. We propose the development of polymer nanocomposite materials embedded with high permittivity nanofillers to obtain high permittivity dielectric materials. Previously, ceramic dielectrics based on highly polarizable materials, such as calcium copper titanates, [1] have been employed for pulse power applications. Although ceramic dielectric materials possess high dielectric constants, their breakdown strength is low [2]. Further, it is hard to manufacture ceramic-based capacitors, whereas polymers can be easily processed into large-area films.

This chapter specifically discusses the shortfalls of the approaches used in the past to

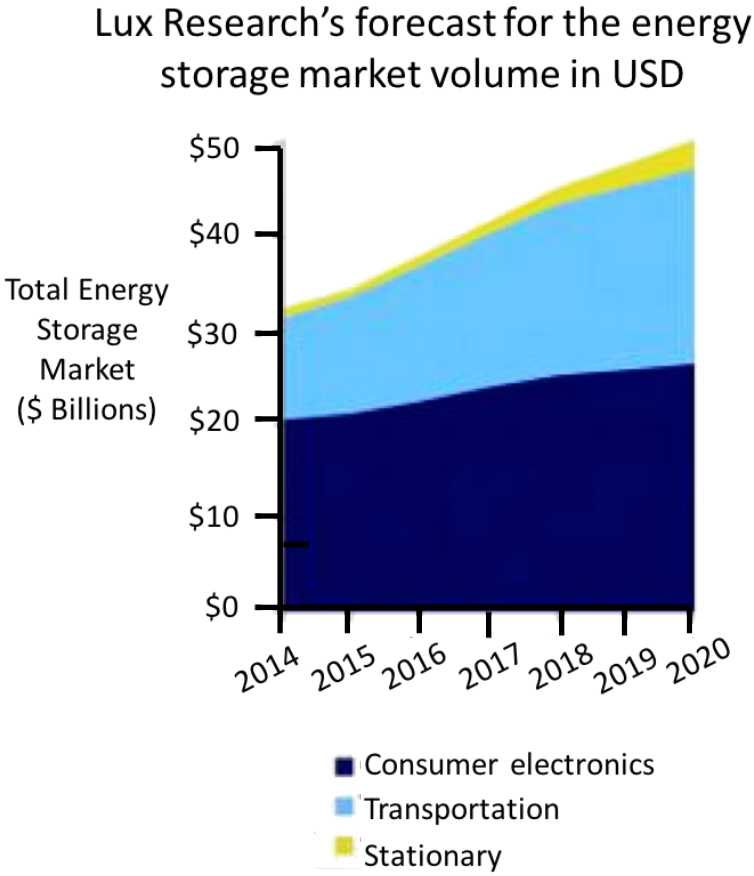


Figure 1.1: Trends in the energy storage market [3].

enhance the dielectric permittivity of the polymer composite materials and the motivation for using appropriate surface functionalization on the nanoparticle surface to overcome these limitations. In addition, the significance of sub-10 nm size fillers over the microsized fillers, and the fundamental working principles of polymer nanocomposite materials are discussed.

## 1.1 Polymer Nanocomposite Dielectrics

Nanocomposite materials are widely used in the areas of photonics, electronics, catalysis, energy storage, and biotechnology [4–10]. Particularly, polymer composite materials with high permittivity, high breakdown strength, low dielectric loss, and good processability are of great interest because of their various applications in energy storage, capacitors, and actuators [11, 12]. Solid-state dielectric materials with high permittivity and high breakdown strength would be an excellent candidate for future energy storage devices.

Polymers offer high breakdown strength, ease of processing, and low dielectric loss, but their dielectric constant is low. Typically, high permittivity fillers such as conductive and ferroelectric fillers [barium titanate ($BaTiO_3$), lead zirconate titanate (PZT)] are embedded in polymers to enhance their permittivity [13–15]. Ideally, the enhancement in dielectric constant should be attained without any comprise in dielectric loss or/and breakdown strength, which entails a uniform dispersion of nanoparticles in the polymer matrices without particle agglomeration and phase separation. However, the dispersion of nanoparticles in polymer matrices is usually challenging, because nanoparticles tend to aggregate or phase-separate.

Table 1.1: Dielectric properties of polymer composites as reported in the literature

| | Filler Material | Dielectric Constant | Energy Density (J/cc) | Reference |
|---|---|---|---|---|
| Ferroelectric Filler Composites | Barium Strontium Titanate | 18 | 14.86 | Tang *et al.*, Nanoletters, 2013 [16] |
| | Barium Titanate | 70 | 10.48 | Haixiong *et al.*, Adv. Energy. Mat., 2013 [17] |
| Conductive Filler Composites | Silver (Ag) | 500 | — | Shen *et al.*, Adv. Mat., 2007 [18] |
| | Nickel (Ni) | 800 | — | Nan *et al.*, Ann. Rev. of Mat. Res., 2010 [19] |

## 1.2 Background

Conductive particles mainly in the form of aggregates were used as fillers in polymers [19–23]. Although extremely high k values were reported for composites near percolation, the dielectric loss was significant [19–23]. A similar trend in the dielectric loss was reported for composite materials containing ferroelectric materials such as $BaTiO_3$ and PZT [13–15]. High dielectric loss and low breakdown strength can be attributed to the poor dispersion of nanoparticles in polymer matrices. Recently, results have been reported for $BaTiO_3$-based nanocomposites, indicating the enhancement in dielectric permittivity with low dielectric loss values ($0.03-0.15$) [24–27]; however, these systems suffer from limited energy storage capacity due to the low saturation voltage of the fillers used [28]. In contrast, conductive-filler-based composites do not suffer from such disadvantages and can enhance the dielectric permittivity significantly [29–31]. However, the particle surface still needs to be passivated

with suitable ligands [32–34] to minimize dielectric loss. Therefore, particle dispersion without agglomeration is imperative to achieve an optimal enhancement in dielectric properties, regardless of the choice of filler material.

## 1.3 Nanocomposite Dielectric Concepts

### 1.3.1 Working Principle

Under an electric field, metal nanoparticles will polarize as shown in Figure 1.2, leading to space charge accumulation at the nanoparticle-polymer interface which results in higher permittivity. Due to the difference in the relaxation times of the two phases, charges get accumulated at the particle-polymer interface, until the charges are relaxed by tunneling (in the case of particle separation within the tunneling range) or by ohmic conduction (in the case of direct particle contact). This interfacial polarization mechanism also known as Maxwell-Wagnar gives rise to the increase in the dielectric permittivity at low frequencies. In addition, the ligand coating on the nanoparticle surface provides local electrical resistance, so these nanoparticles could still be incorporated at a high volume ratio in the polymer scaffold without compromising the breakdown strength and causing an increase in the dielectric loss of the polymer nanocomposite. This is in contrast to the previous studies where a significant enhancement in the dielectric permittivity was obtained on the the addition of the conductive fillers to the polymer matrix but at a high dielectric loss and reduced breakdown strengths. The interfacial ligand/surface functionalization layer can restrict the electron transfer between the nanoparticles, resulting in a more gradual increase in the dielectric permittivity with the increase in nanoparticle concentration.

Nanometric-sized high dielectric constant particles are particularly attractive candidates for their use as fillers in dielectric nanocomposite materials [35, 36]. It has been indicated that dielectric properties can be enhanced (controlled) by an interfacial interaction between

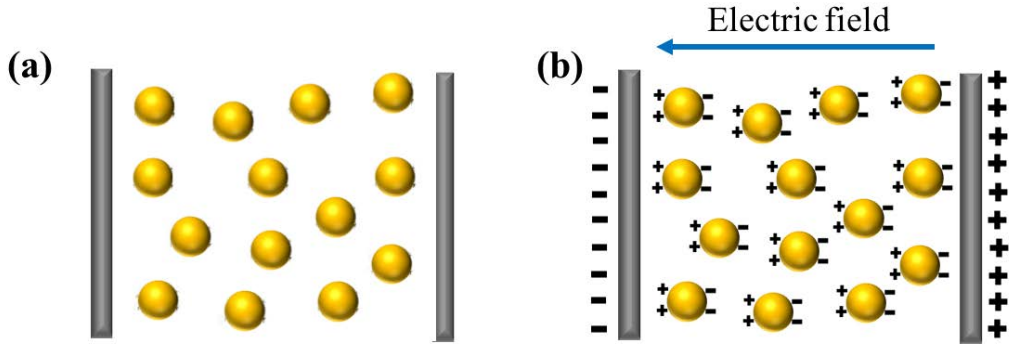


Figure 1.2: Metal nanoparticles embedded in a polymer matrix (a) in the absence and (b) in the presence of an electric field.

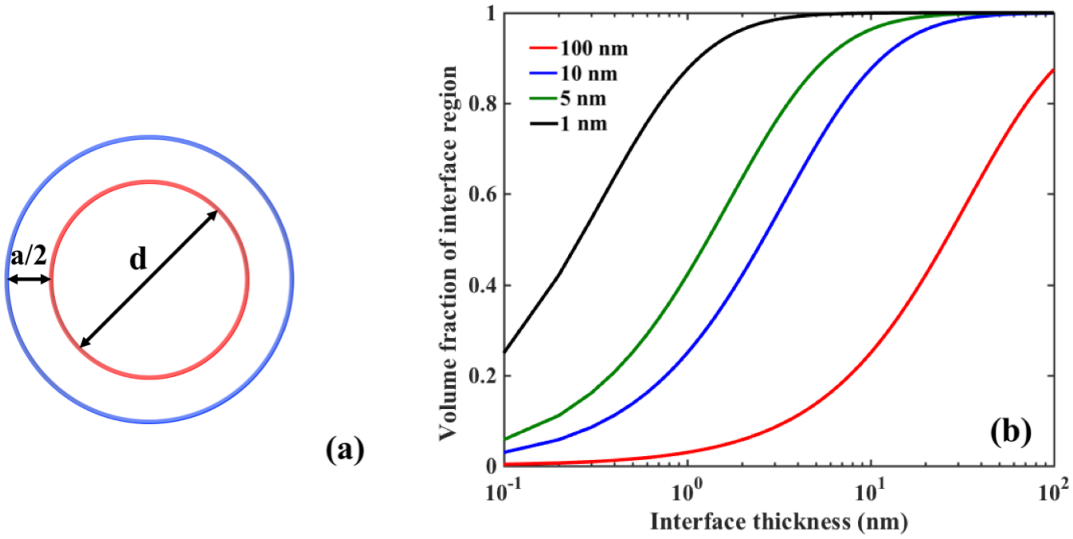


Figure 1.3: (a) Spherical geometry is assumed for the interface volume calculations relating particle diameter d, interface thickness a, and the interface volume fraction. (b) Interface volume fraction as a function of interface thickness for 1, 5, 10, and 100 nm particles.

particles and polymers as particles size decreases to nanoscale [35–39]. Figure 1.3 shows the variation of the interface volume fraction with the interface thickness for different particle sizes [9,53]. Spherical geometry is assumed for the interface volume calculations relating particle diameter (d), interface thickness (a) and the interface volume fraction. It should be noted that the interface volume fraction exceeds 0.5 of the whole particle volume for the particle diameter less than 5 nm and the interface thickness of 1 nm [35, 36]. Therefore, the nanoparticles/matrix interfaces can significantly affect the physical, mechanical, and electrical properties of nanocomposites [35–39]. In particular, Putson *et al.* [40] observed that the enhancement in the effective dielectric permittivity was more obvious in case of nano-sized copper particles compared to the micro-sized particles. Furthermore, the size of the nanoparticles could significantly affect their distribution in the host polymer matrix [41, 42]. In general, nanoparticles with size comparable to the radius of the gyration of the host polymer chains can facilitate favorable particle-polymer interactions [41]. The effect of particle size on their state of dispersion in polymer is discussed in detail in Chapter-2.

### 1.3.2 Dielectric Permittivity

Electrical energy can be stored in the form of charge separation in dielectric materials, when the charge distributions around the constituent atoms or molecules are polarized under an external electric field. The complex permittivity of a material is defined as:

$$\epsilon^* = \epsilon^{'} - j\epsilon^{"} \tag{1.1}$$

where $\epsilon^{'}$ and $\epsilon^{"}$ is the real and imaginery parts of the complex permittivity. The magnitudes of $\epsilon^{'}$ and $\epsilon^{"}$ depend on the frequency of the applied electric field. The real part of the electric permittivity is defined as:

$$\epsilon^{'} = \epsilon^{o}\epsilon^{r} \tag{1.2}$$

where $\epsilon^{r}$ is the relative permittivity and $\epsilon^{o}$ is the permittivity of the free vacuum. For a parallel plate capacitor containing a dielectric material with area $A$ and thickness $d$, the capacitance is given by:

$$C = \epsilon^{o}\epsilon^{r}A/d \tag{1.3}$$

As the polarization of a material under an electric field varies, part of the field energy is dissipated due to conduction or conversion into thermal energy. Loss tangent measures the energy dissipated by the dielectric in an oscillating electric field. It is defined as the ratio of the imaginery and real parts of the permittivity. Ideally the loss tangent should be zero, since we want to minimize the dielectric losses in a energy storage device such as capacitor.

$$tan\delta = \epsilon^{"}/\epsilon^{'} \tag{1.4}$$

### 1.3.3 Breakdown Strength

The energy stored in a capacitor is expressed as:

$$W = (1/2)CV_{bd}^{2} \tag{1.5}$$

where $V_{bd}$ is defined as the breakdown voltage of the dielectric material. The above expression can be reformulated in terms of the relative permittivity as:

$$W = (1/2)\epsilon_{o}\epsilon_{r}AdE_{bd}^{2} \tag{1.6}$$

where $E_{bd}$ is defined as the breakdown field strength. Equation 1.6 implies that the dielectric permittivity and dielectric breakdown strength should be enhanced simultaneously to realize high capacity energy storage.

Polymer nanocomposite dielectrics are limited by the amount of the voltage they can withstand prior to their electrical and chemical breakdown. The maximum applied electric field strength that a dielectric can withstand is defined as the dielectric breakdown strength. In polymers, there are there mechanisms of breakdown; electronic, thermal and mechanical processes [43]. In general, the dielectric breakdown in polymers is attributed to the electronic avalanche mechanism via the formation and propagation of electrical trees in the dielectric film [44–46]. Structural defects in the film are the primary cause of the formation of electrical trees that eventually propagates between the top and the bottom electrodes leading to breakdown. The thermal breakdown process is initiated by the steady state or impulse thermal processes at high temperatures, and above a certain critical temperature, an electromechanical mechanism dominates the breakdown behavior. The electrostatic forces between the electrodes cause deformations and softening of polymers resulting in an electromechanical breakdown of the dielectric.

## 1.4 Thesis Outline and Description

This introductory chapter has provided the motivation and background in polymer nanocomposite dielectric materials. The next chapter covers the fundamental approaches used for controlling particle dispersion in polymer, and the material selection strategies for the nanocomposite design. This chapter also discusses the nanoparticle and polymer materials that were selected for the nanocomposite design and development. The third chapter focuses on the experimental methods used for nanocomposite synthesis, material, and electrical characterization. Chapter 4 reports on the design and development of a photodefinable gold nanoparticle/SU-8 polymer nanocomposite for potential applications in embedded capacitors. This chapter begins by describing the nanoparticle synthesis protocol, followed by the detailed characterization of the nanocomposite film morphology, nanoparticle dispersion in the polymer matrix and the dielectric properties. The fifth chapter focuses on the development of gold nanoparticle/PVDF nanocomposite dielectric. This includes optimization of the process conditions to obtain dielectric films with reduced voids, selection of appropriate ligands to prevent nanoparticle agglomeration, detailed characterization of the particle dispersion under varied particle volume fractions. The chapter concludes with an evaluation of the overall enhancement in the dielectric properties. The sixth chapter summarizes the dissertation and the last chapter examines the areas for future research.

# Chapter 2

# Material Design

This chapter discusses the factors affecting the distribution and agglomeration of nanoparticles in the polymer matrices, material selection strategies used for selecting the polymer and nanoparticle materials, and the individual components of the polymer nanocomposite systems considered in this dissertation. To reduce the dielectric loss and the reduction in the breakdown strength, it is important to minimize the particle agglomeration and to obtain a uniform particle dispersion. Hence, the nanoparticle surface functionalization/ligand should be selected so as to promote favorable interactions between the particles and polymer.

A nanocomposite dielectric consists of a high permittivity phase such as nanoparticles/nanorods/nanoplatelets embedded inside a polymer phase. Typically, the dispersion of nanoparticles in polymer matrices is problematic and the nanoparticles tend to phase separate or aggregate in the polymer matrix. The interaction of nanoparticles with the polymer phase is mediated by the ligands attached to the nanoparticle surface. Hence, the ligands play a significant role in controlling the particle dispersion and spatial distribution in the polymer matrix. Owing to the complex physical and chemical interactions between the various components (Figure 2.1), the optimization of material selection is not obvious. Moreover, it is challenging to predict the phase stability of the nanoparticle polymer blends due to the computational difficulty in accessing the relevant length and time scales.

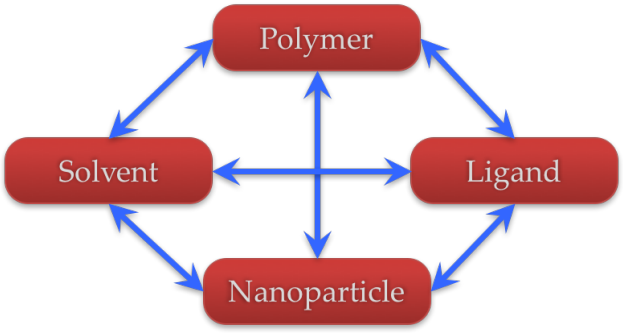


Figure 2.1: Interactions among the various components of a polymer nanocomposite system.

## 2.1 Nanoparticle dispersion in polymer matrices

In nanoparticle polymer composite systems, although enthalpic interactions (related to the nanoparticle ligands) are usually dominant [47], [41], entropic interactions (i.e. size of the nanoparticles relative to the radius of gyration of polymer) can also play a critical role in controlling the nanoparticle dispersion.

### 2.1.1 Nanoparticle Surface Functionalization

Through surface modification of nanoparticles, it is possible to vary the enthalpic interactions in the nanoparticle polymer system. To achieve repulsion in polymer composite systems, functional small molecules or polymers are attached to the nanoparticle surface by physical adsorption or covalent bonding. Synthesis of nanoparticles coated with small molecule ligands usually involve decomposition of the organometallic precursors in a solution environment. Examples include alkane based ligands such as alkyl thiols, phosphine oxides, amines. The direct mixing of such nanoparticles with most polymers leads to nonuniform distribution and aggregation. To obtain uniform dispersion, these conventional ligands are replaced with ligands that favorably interact with the host polymer.

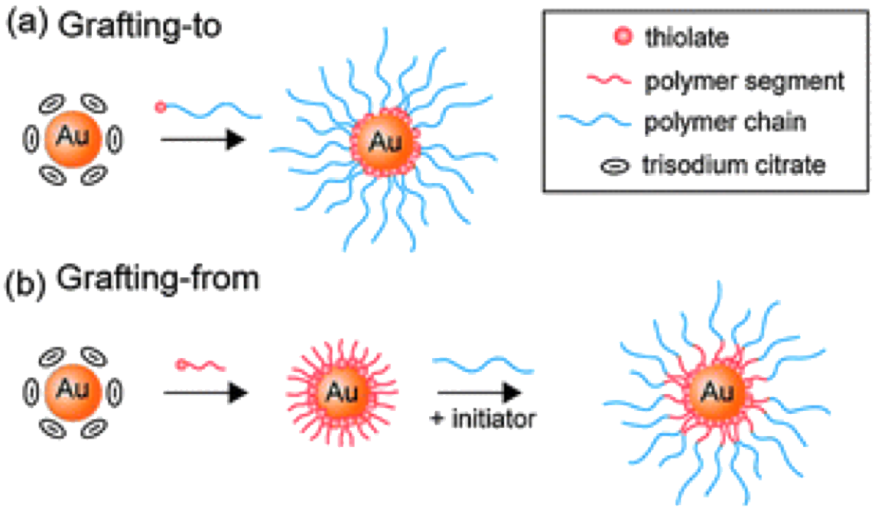


Figure 2.2: Scheme showing the polymer grafting strategies on nanoparticle surface [48].

Synthesis of polymer-coated nanoparticles is accomplished by either "grafting to" and "grafting from" methods. The "grafting to" technique involves performing the particle synthesis in the polymer matrix, replacing the ligands inherent to nanoparticle synthesis with the end-functionalized polymer molecules. According to "grafting from" technique, growth of polymers is initiated from the nanoparticle surface by the attached (usually covalent bonded) initiating groups. For example, Figure 2.2 illustrates the polymer grafting strategies on the gold nanoparticle surface. Figure 2.2 (a) shows the replacement of the trisodium citrate

capping molecules with polymer grafts. In Figure 2.2 (b), the polymers are grown from the nanoparticle surface via polymerization reaction.

### 2.1.2 Wetting Characteristics

Since the nanoparticles are solids, the polymer chains must stretch around these obstacles, causing a loss in the conformational entropy that increases with the particle radius [49]. In the absence of specific interactions, larger nanoparticles are expelled from the bulk of the polymer, whereas smaller particles are not. This significantly affects the global distribution of nanoparticles in the polymer matrix.

In case of polymer coated nanoparticles, for wetting to be favored entropically, either the particle size must be lower than the radius of gyration ($R_g$) of the matrix polymer [41] (viable only for very small nanoparticles, in general), or the size of the brush polymer must be no less than the matrix polymer size [50, 51]. If the brush polymers are appreciably smaller than those of the matrix polymer, entropy gained due to mixing of brush and matrix is less than entropy lost by the matrix chains when penetrating the brush layer. This discrepancy results in the brush being excluded from the matrix, leading to particle aggregation, as shown in Figure 2.3. Due to low entropy of mixing in polymers, the brush must be either miscible with or chemically identical to the matrix polymer so that dispersion is not enthalpically disfavored. For a multilayer system where a layer of poly(methyl methacrylate) (PMMA) containing poly(ethylene oxide)-coated CdSe particles is in contact with a brittle silicon oxide layer, the nanoparticles with size comparable to the radius of gyration (Rg) of host PMMA were found to migrate in the crack in silicon oxide layer [52]. This crack was induced upon heating the multilayer system above the glass transition temperature of the composite [52].

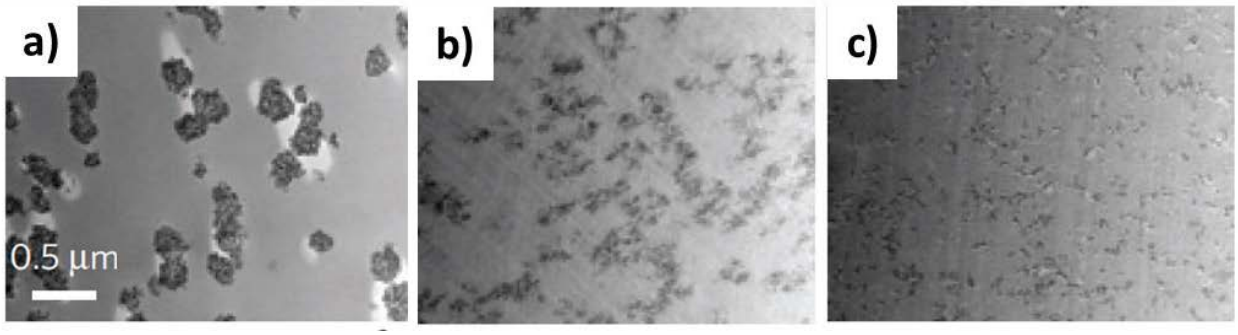


Figure 2.3: Effect of brush molecular weight on the dispersion of PS-grafted silica (14 nm diameter, 0.01 chains/nm$^2$ graft density) in a 42 kg mol$^{-1}$ PS homopolymer matrix. Brush polymer molecular weight: a) 25 kg mol$^{-1}$($< MW_{matrix}$), b) 51 kg mol$^{-1}$($\approx MW_{matrix}$), c) 158 kg mol$^{-1}$($> MW_{matrix}$). [53]

## 2.2 Material Selection

### 2.2.1 Polymers

We considered high breakdown strength polymers based on literature as shown in Figure 2.4, and evaluated them against four key parameters namely breakdown strength, solubility, compatibility, and the ease of thin film fabrication. Here, solubility is defined as the ability of the chosen polymer to be dissolved in various organic solvents, and compatibility means the extent to which the polymer solvent is compatible with the solvent in which nanoparticles are dispersed. It is worth noting that a solution-mixing approach is used for the synthesis of the polymer nanocomposite material that involves mixing of a nanoparticle solution with the polymer solution. Hence, solubility and compatibility parameters are considered for polymer selection in addition to the polymer breakdown strength and the ease of film fabrication. The solubility of polymers was analyzed in various organic solvents. Figure 2.4 shows that polycarbonate and polypropylene have high breakdown strength and good solubility, but lack of compatibility with the nanoparticle solvent rules them out. Based on breakdown strength, solubility and compatibility parameters, PVDF would be an ideal choice. However, since we need to fabricate these films from solution, we also considered ease of film fabrication and hence, selected SU-8 as well. Furthermore, SU-8 is a photodefinable polymer and would be useful for embedded capacitor applications that require photopatternable high dielectric permittivity dielectrics.

| | Polymer Dielectric Materials | | | | |
|---|---|---|---|---|---|
| Property | SU-8 | Polycarbonate (PC) | Polyester (PET) | Polyvinylidene fluoride (PVDF) | Polypropylene (PP) |
| Breakdown Strength (MV/m) | 440 | 528 | 570 | 590 | 640 |
| Solubility | Good | Good | Bad | Good | Good |
| Compatibility | Good | Bad | Bad | Good | Bad |
| Ease of Film Fabrication | Good | Bad | Bad | Bad | Bad |

Figure 2.4: Selection of the host polymer matrix [54–56]

#### 2.2.1.1 SU-8

SU-8 is a well-established epoxy which is commonly used in microfabrication. The physical properties of SU-8 are listed in Table 2.1. It can be inferred that SU-8 has been a very comprehensively investigated material. In addition to the listed properties, SU-8 has good stability at elevated temperatures and resistance to moisture and solvents, implying that it wouldn't swell or/and dissolve in solvent exposing environments. SU-8 also has high glass transition and degradation temperatures.

Table 2.1: Summary of important properties of SU-8

| **Characteristics** | **Value** | **Conditions** | **Reference** |
|---|---|---|---|
| Density | 1190 Kg/m$^3$ | Raw SU-8 resin | [57] |
| | 1218 Kg/m$^3$ | Fully cross-linked | [58] |
| Melting Point | 82°C | Raw SU-8 | [59] |
| Polymer shrinkage | 7.5% | Post-baked at 95°C | [60] |
| Glass transition temperature | 50°C | Unexposed film | [61] |
| | $>$ 200°C | Fully cross-linked film | [61] |
| Degradation temperature | 380°C | Fully cross-linked | [61] |
| Volume resistivity | $(1.8 - 2.8) \times 10^{14}\Omega$m | Hard-baked at 150°C | [62] |
| Surface resistivity | $(5.1 - 18) \times 10^{14}\Omega$m | Hard-baked at 150°C | [62] |
| Dielectric constant | 4 | Post-baked at 100°C; 20 GHz | [63] |
| | 4.5 | at 10 MHz | [63] |
| | 5.07 | Hard-baked at 150°C; 1 MHz | [59] |
| Loss tangent | 0.14 | at 1 THz | [64] |

SU-8 is composed of Bisphenol A Novolak epoxy oligomer that is dissolved in an appropriate organic solvent and the photoinitiator (usually from triarylsulfonium salts family) to crosslink SU-8. When exposed to light, a photochemical reaction takes place producing an acid which acts as catalyst in the cross-linking reaction. In order for the cross-linking to take place, post exposure bake must be done above the glass transition temperature of SU-8.

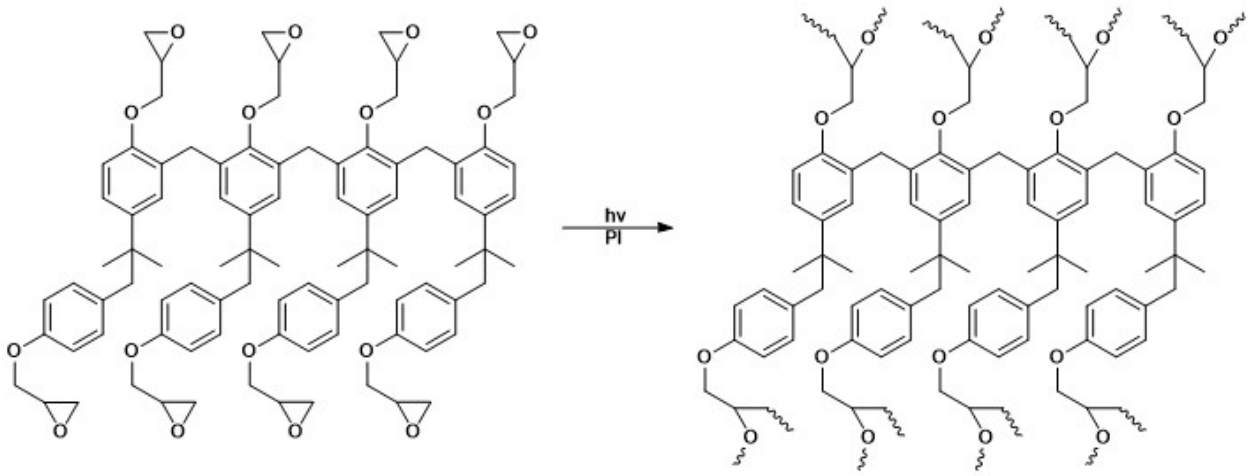


Figure 2.5: Molecular structure of SU-8 monomer. There are eight epoxy groups in the monomer, which justifies the number ′8′ in the name (SU-8).

The molecular structure of the SU-8 monomer before and after cross-linking is shown in Figure 2.5(a) and (b). The number ′8′ in the polymer name (SU-8) can be assigned to the number of epoxy groups in the oligomer. Bisphenol A Novolak epoxy oligomer also known as EPON Resin SU-8 is commercially available in the granular form and is manufactured by Momentive Specialty Chemicals Inc.

#### 2.2.1.2 PVDF

Poly(vinylidene fluoride) (PVDF) is a thermoplastic fluoropolymer with excellent chemical resistance, high mechanical strength and thermal stability [65–69]. It is widely used in dielectric applications because of its high dielectric constant (8-10) [70], and high breakdown strength. The physical properties of PVDF are listed in Table 2.2. PVDF is a semi-crystalline polymer with four crystalline forms: the nonpolar $\alpha$ and the polar $\beta, \gamma$ and $\delta$ forms [71, 72]. The most common polymorph is the nonpolar $\alpha$ phase, the dipole moments of $\alpha$ crystallites are oriented in opposite directions resulting in a zero net polarization. The highest dipole moment is obtained when all the dipoles are aligned in the same direction, corresponding to the $\beta$ phase of PVDF. The $\alpha$ and $\beta$ conformations are shown in Figure 2.6.

### 2.2.2 Nanoparticles

Conductive particles are used as nanofillers with the aim of enhancing the dielectric permittivity of the host polymers. In particular, gold nanoparticles are promising candidates for polymer nanocomposites due to their ease of functionalization with a variety of capping ligands such as alkyl thiols, phosphine oxides, amines, and polymer brushes. Moreover, gold

nanoparticles can be easily synthesized in large volumes with precise size control/tight size tolerances.

Table 2.2: Important properties of PVDF [73]

| **Properties** | **Values** | **Conditions** |
|---|---|---|
| Density | 1780 Kg/m$^3$ | at 25°C |
| Melt flow | 7-20 g/10 min | (230°C/12.5kg) |
| Melting point | $166 - 170$°C | ASTM D 3418 |
| Glass transition temperature | $-30$°C | DMTA |
| Viscosity | 17500-21500 poise | (230°C) (100 sec$^-$1)(lit.) |
| Hardness | 76-80 | (Shore D, ASTM D 2240) |
| Impact strength | 2-4 ft-lb/in. | (Izod, ASTM D 256) |
| Dielectric constant | 8-9.5 | at 100 Hz (ASTM D 150) |

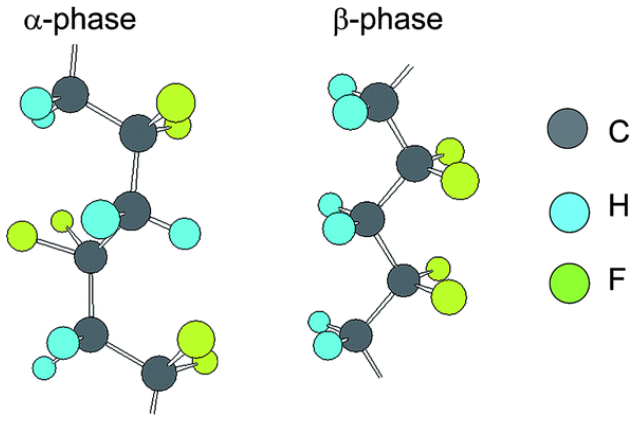


Figure 2.6: Structure of the $\alpha$ and the $\beta$ phase of PVDF [74].

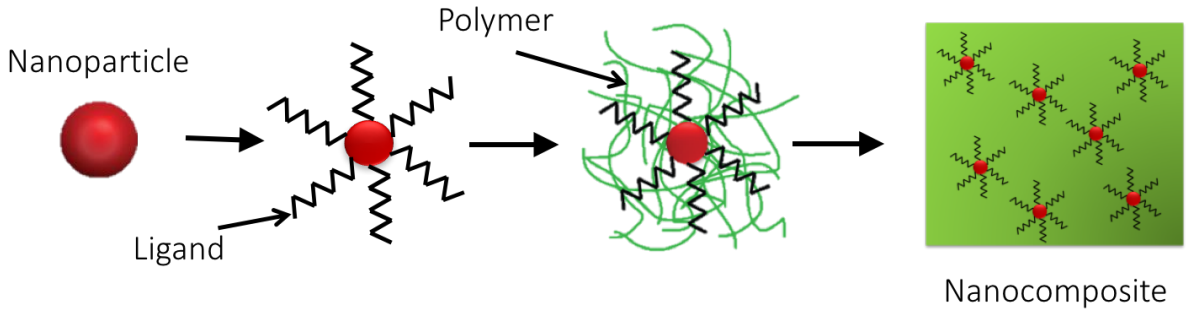


Figure 2.7: Components of a polymer nanocomposite system

| Components | Gold nanoparticle / SU-8 nanocomposite | Gold nanoparticle / PVDF nanocomposite |
|---|---|---|
| **Polymer** | SU-8 | PVDF |
| **Solvent** | Chloroform | Dimethylformamide (DMF) |
| **Nanoparticle (NP)** | Gold nanoparticle (6.32 ± 0.56 nm) | Gold nanoparticle (4.5 ± 0.6 nm) |
| **NP surface functionalization/Ligand** | Dodecanethiol | Polyvinylpyrrolidone (PVP) |

Figure 2.8: Components of the gold nanoparticle/polymer nanocomposite systems.

## 2.3 Polymer Nanocomposite Systems

Nanoparticle, polymer and ligands (nanoparticles' surface functionalization) are the components of a polymer nanocomposite system (Figure 2.7). Ligands are molecules which are physically or chemically bonded onto the nanoparticle surface to prevent the nanoparticle agglomeration, which is a major issue due to the high surface area of nanoparticles. The solubility of SU-8 and PVDF was analyzed in various solvents and based on experiments,

chloroform and dimethylformamide was selected for SU-8 and PVDF respectively. For the selected SU-8 and PVDF polymers, nanoparticle surface functionalization groups were appropriately chosen to facilitate favorable interactions between the particles and polymer. Figure 2.8 shows a list of the components of each of the SU-8 and PVDF polymer nanocomposite systems.

# Chapter 3

# Experimental Techniques

In this chapter, first the methods for synthesizing nanocomposite materials, their advantages and limitations are discussed. The range and the specificity of the nanocomposite materials that can be synthesized could vary from one method to another. Hence, it is important to understand the basic principles involved in the synthesis approaches for making the right selection. Next, thin film deposition methods, and material characterization techniques used to study the particle agglomeration in polymer and the morphology of the nanocomposite films is discussed. The last part of the chapter concerns the fundamentals and the testing procedure employed for the dielectric permittivity and the breakdown strength measurements.

## 3.1 Nanocomposite Synthesis and Processing Techniques

### 3.1.1 Synthesis

There are three general methods for the fabrication of nanocomposites as discussed below.

#### 3.1.1.1 In Situ Polymerization Method

The first method involves the in situ polymerization in the presence of nanofillers. In this method, the fillers are embedded in a monomer solution and the resulting mixture is polymerized [75–78]. Figure 3.1 shows a schematic of the in situ polymerization method. The key to this technique is the homogeneous dispersion of the fillers in the monomer, which might necessitate functionalization of the nanofiller surface to improve the wetting of the nanofillers by the polymers.

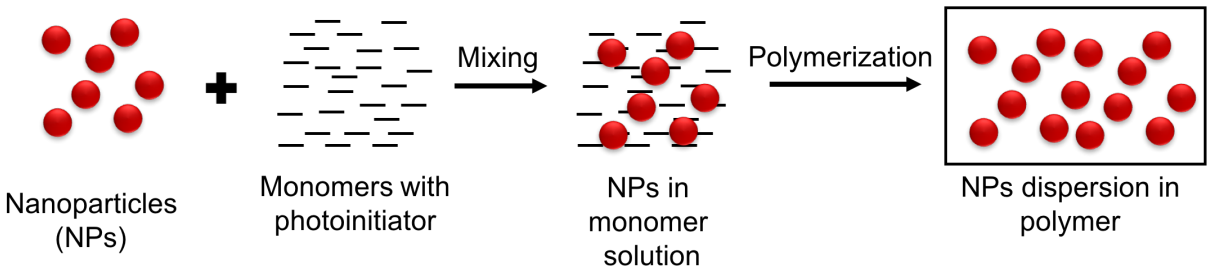


Figure 3.1: A scheme for the in-situ polymerization nanocomposite synthesis method.

#### 3.1.1.2 Sol-Gel Method

The second method includes the in situ formation of the nanofillers and the in situ polymerization. This is a bottom-up approach that typically employs the reaction of the metal alkoxides [79–85]. For example, equation 3.1 shows the sol-gel reaction used for the synthesis of the silica/polymer molecular composite materials.

$$Si(OR)_4 + 4H_2O[Si(OH)_x(OR)_{4-x} + xROH]SiO_2 + 4ROH + 2H_2O \tag{3.1}$$

This approach is limited to polymers having hydrogen bond acceptor moieties that can bind to the hydroxyl groups on the inorganic naofiller surface via hydrogen bonding, for example: nanoparticles with alcohol group on their surface and water soluble polymers. In addition, the dispersion of the nanofillers in the polymer is dictated by the experimental conditions of the sol-gel reactions. Due to the limitation in the selection of the polymers and the difficulty involved in the synthesis of composite materials with stable quality, usage of this approach is fairly limited.

#### 3.1.1.3 Direct Mixing of Nanoparticles and Polymers

The third method involves the direct mechanical mixing of the nanofillers and the polymer. Nanofillers and polymers can be directly mixed in two ways. The first one involves mixing a polymer with the nanofillers in the absence of solvents, also referred to as the melt-compounding method (Figure 3.2). In the second method, also called solution-mixing (Figure 3.3), the nanofillers and polymers are mixed as in a solution.

In the melt-compounding method [86–90], shear stresses induced in the polymer melt during melt compounding cause the breakdown of the filler aggregates to nano-scale. Therefore, the shear stresses primarily governs the dispersion of the nanofillers in the polymer matrix. In the solution-mixing method, the nanofillers are dispersed in a pre-synthesized polymer solution to prepare the nanocomposite solution, followed by the evaporation of the solvent from the nanocomposite solution [91–95]. The shear forces induced in the nanocomposite solution during the mixing process are much lower and hence, the dispersion of nanofillers in the polymer relies on the external factors such as surface functionalization of the nanofillers/nanoparticles [93, 94]. Unlike in situ polymerization, and sol-gel methods,

this method provides full synthetic control over both nanoparticles and polymer and has the potential of generating a wide variety of composite materials. In this work, solution-mixing approach is adopted for the synthesis of the nanocomposite material.

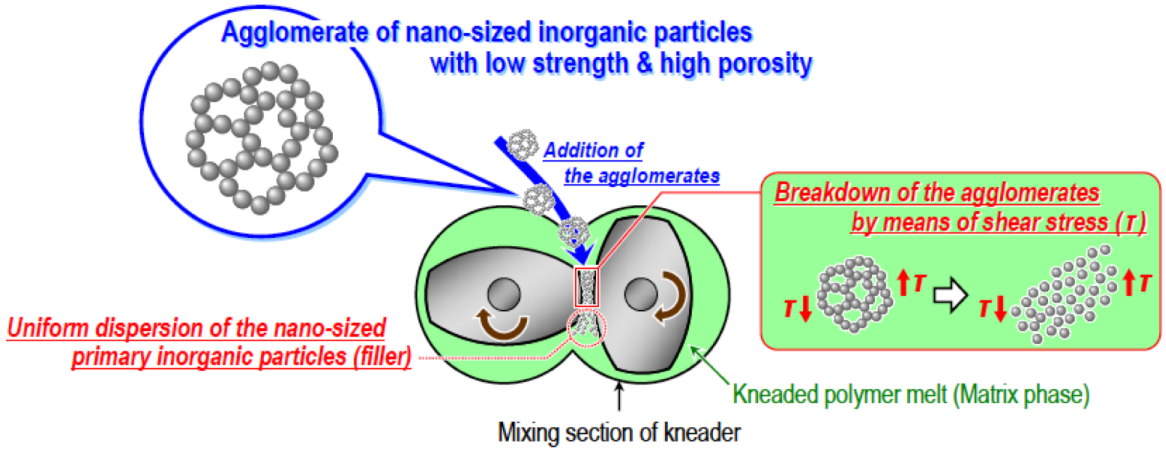


Figure 3.2: A schematic of the fabrication of polymer nanocomposites by the melt-compounding method [96].

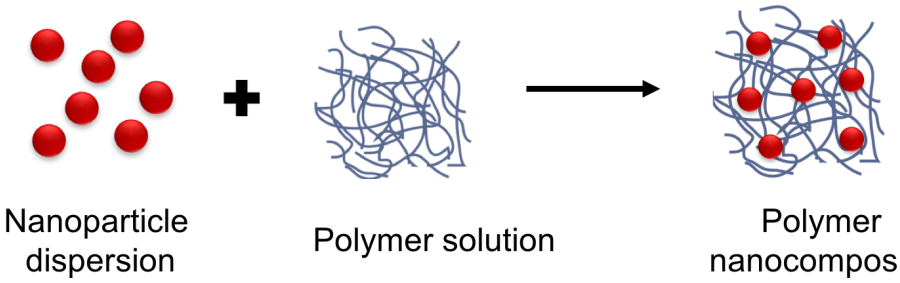


Figure 3.3: A conceptual illustration of the synthesis of nanocomposites using solution-mixing method.

### 3.1.2 Thin Film Deposition

For the deposition of thin films from solutions several approaches have been developed namely solution casting, spin coating, doctor blade coating, and dip coating. Out of these approaches solution casting and spin coating are used more frequently. Solution casting involves dropping the nanocomposite solution on the substrate and subsequently, allowing the solvent to evaporate. In the spin coating method (Figure 3.4 ), first the solution is dropped onto the

substrate followed by spinning the substrate at a certain rotation speed for a certain amount of time.

Spin casting method results in a much more uniform film thickness than solution casting. The final film thickness depends on the viscosity of the solution, rotation speed, and time. Too high of a speed or too long of a spin time can result in much faster evaporation of solvent. This can minimize the film thickness but can also result in poor quality films. Too slow of a speed or too short of a spin time can result in uneven spreading of the solution across the substrate, resulting in non-uniform films. Therefore, a balance must be achieved in order to deposit films well on the substrate.

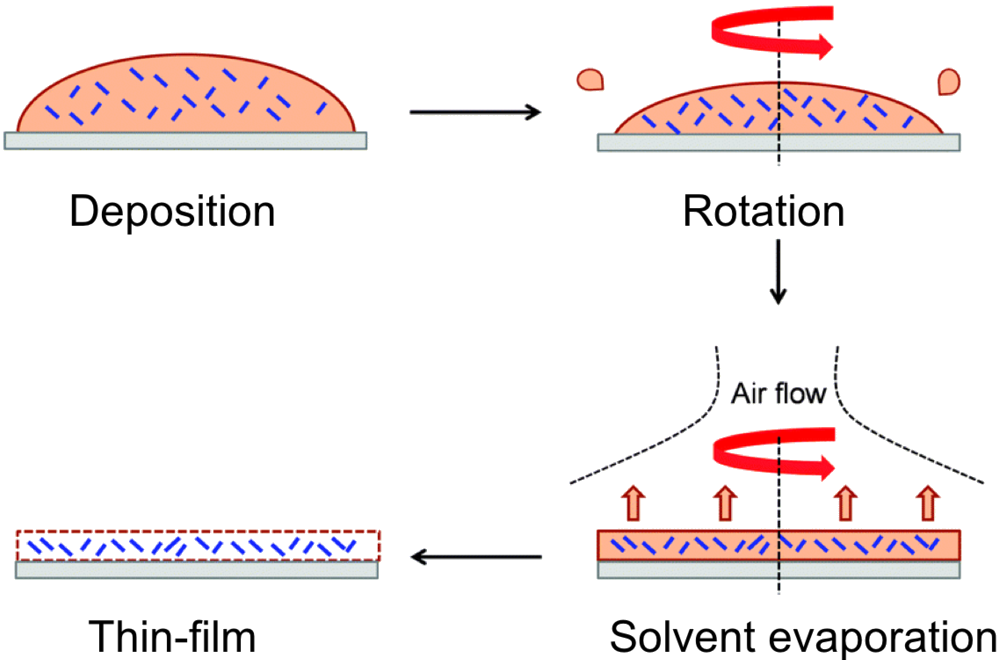


Figure 3.4: A schematic to illustrate the spin coating process [97].

Dip coating is a commercially used wet thin film deposition method. In the dip coating method, first the substrate is immersed into the polymer/nanofiller solution at a constant speed followed by a dwell time to allow sufficient interaction of the substrate with the solution. Then, the substrate is pulled upward at a constant speed to obtain a thin layer of the coating solution, the excess liquid solution will drain from the surface. Finally, the solvent evaporates from the coated layer, forming as-deposited film. Figure 3.5 shows a schematic of the dip coating process. The resulting film can be subjected to further heat treatment process if needed. The dip coating method offers the advantage of good uniformity, large area processing, and very low film thickness. However, this process is time consuming, and the wastage of the material is a concern.

Doctor blade coating is widely used in paper, photographic film, textile and printing industries for large area thin film processing. In this method, a static blade (a metal bar)

applies a unidirectional shear force to the precursor solution that passes through a small gap between the substrate and the blade. Figure 3.6 shows a conceptual illustration of the doctor blade coating process. The advantages of this method are large area coverage, good thickness uniformity and no wastage of material. Doctor blade coating is limited to film thickness > 150-200 nm.

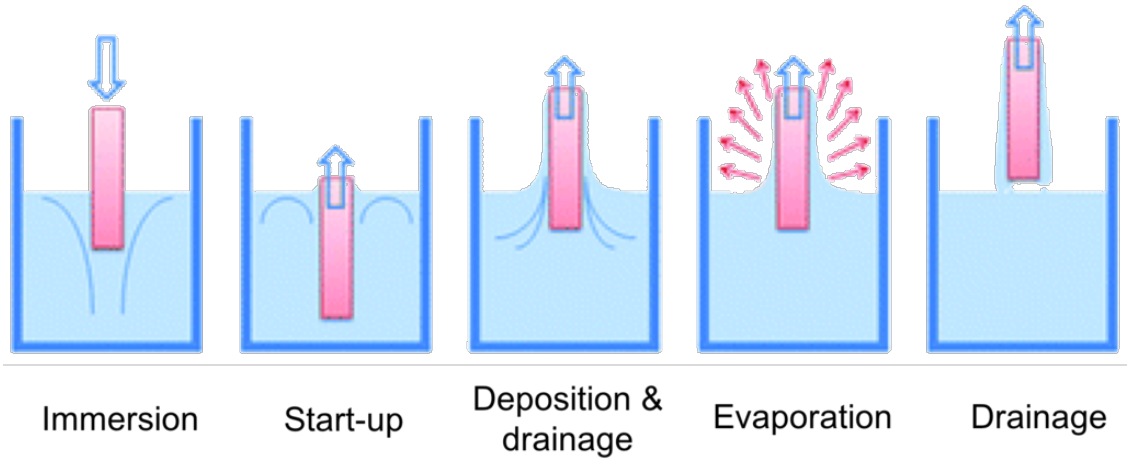


Figure 3.5: Schematic illustration of the dip coating process [98].

## 3.2 Material Characterization

### 3.2.1 Scanning Electron Microscopy (SEM)

A high resolution field-emission Quanta 3D FEG was used to study the surface morphology of the nanocomposite films. A silicon drift detector of size 20 $mm^2$ was fitted to the FEI SEM for carrying out the energy dispersive spectroscopy (EDS) analysis.

### 3.2.2 Microtoming

Nanocomposite film cross-section samples for TEM were prepared using a Reichert-Jung microtome. Nanocomposite film was drop-casted onto an epoxy substrate and then the sample was cut with a diamond knife attached to a boat in which the cut sections float on top of water. The thin slices (40-80 nm) were collected and placed onto the TEM grid for analysis.

### 3.2.3 Transmission Electron Microscopy (TEM)

A FEI Tecnai 12 Transmission Electron Microscope was used for the electron microscopy studies. For nanoparticle imaging, samples were prepared by depositing a drop of the

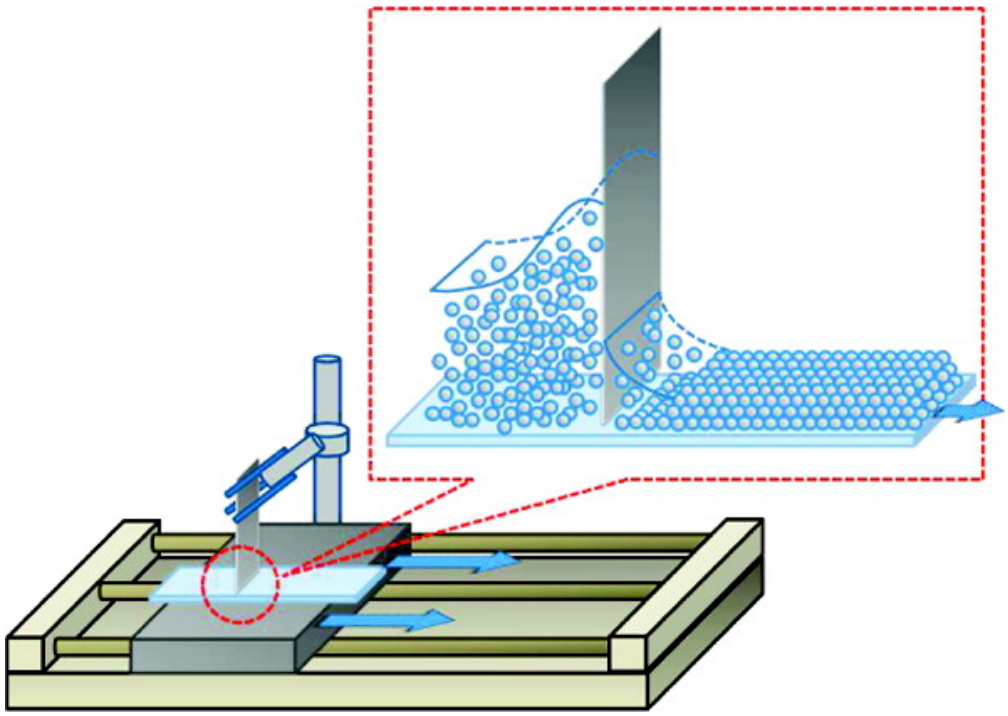

Figure 3.6: Schematic illustration of the doctor blade coating process [99].

nanoparticle suspension on a copper grid covered with holey carbon film. Nanocomposite film samples were prepared by the placing the microtomed cross-sections on the gold TEM slot grids.

### 3.2.4 Grazing Incidence X-ray Diffraction (GIXD)

GIXD measurements were performed on Beamline 7.3.3 at the Advanced Light Source (ALS), Lawrence Berkeley National Laboratory. An X-ray beam impinged onto the sample at a grazing angle above and below the critical angle of the polymer film ($\alpha_c = 0.16$) but below the critical angle of the silicon substrate ($\alpha_c = 0.22$). The wavelength of X-rays used was 1.240 Å, and the scattered intensity was detected by Pilatus 1M detector. The samples were placed in a helium chamber during the measurement to get rid of air scattering. Beam center and the sample-to-detector distance were calibrated using silver behinet. Figure 3.7 shows the experimental setup used for measuring GIXD patterns. Diffraction data was obtained using the Nika software package.

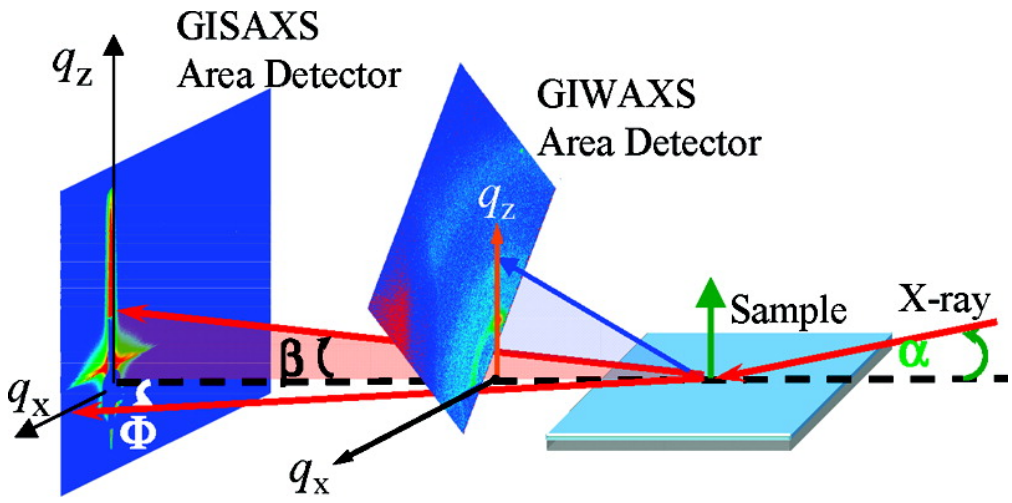


Figure 3.7: Schematic of the setup for synchronized GIXD with the beam incident angle $\alpha$ and the scattering angles $\beta$ and $\phi$ in the out-of-plane (qz) and in-plane directions (qx) respectively. GIWAXS detector plane was normal to the incident beam; the detector was titled 45$^o$C out of the horizontal plane to cover scattering in the qz and qx directions.

## 3.3 Electrical Characterization

Electrical measurements were performed using a probe station (Signatone, model H100) with a blunt tungsten probe tip to minimize mechanical damage to the soft nanocomposite films.

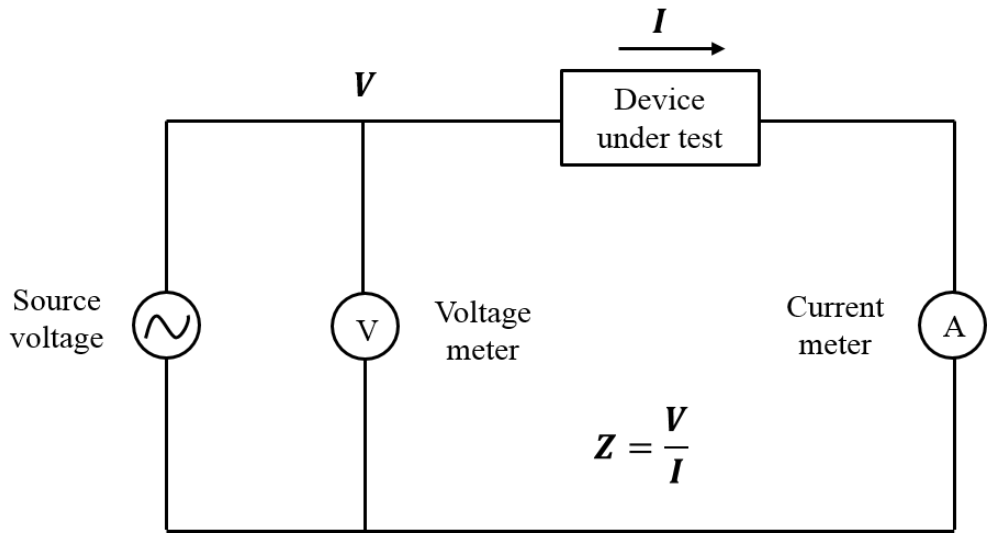


Figure 3.8: Equivalent circuit diagram of the dielectric spectroscopy set-up.

### 3.3.1 Dielectric Spectroscopy

The agilent semiconductor device parameter analyzer B1500A was used for the capacitance measurements. The measured capacitance values were used to calculate the real and the imaginary parts of the permittivity. Figure 3.8 shows a circuit diagram of the capacitance measurement set-up.

The electric permittivity of a material is constant in a DC field in the absence of dielectric saturation. Under an AC field, the permittivity of a material strongly depends on the frequency of the applied electric field and can be expressed in the form of a complex number with a real part $\epsilon'$ and an imaginary part $\epsilon''$. The ratio of the imaginary part to the real part of permittivity $\epsilon''/\epsilon'$, is defined as the dissipation factor (DF) which is also known as the loss tangent ($\tan\delta$) because it is related to the dielectric loss.

Measurement errors could arise due to the stray admittance and residual impedance of the test fixture used. In order to eliminate the measurement errors, calibration was performed in the open and short circuit conditions. The first step to perform a correction on the test system is to apply a short across the probes, typically by setting the two probe heads down on the same contact pad. Then, the capacitance meter measures the impedance value, and stores it as the residual short impedance. The next step is to lift the probes, keeping them in an orientation that approximates where they will be when the actual device is measured. Then the capacitance meter measures the value, and stores that as the residual open impedance.

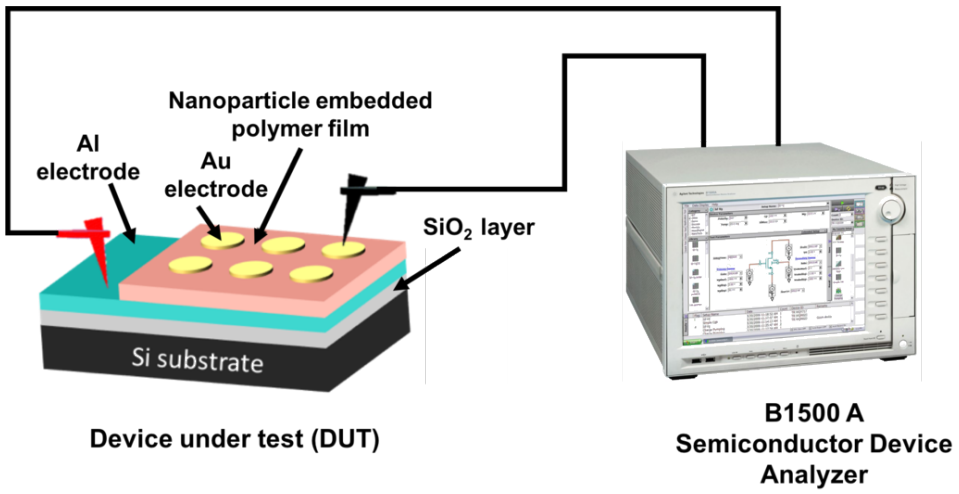


Figure 3.9: Schematic illustration of the experimental set up used to measure the dielectric properties and the breakdown strength.

### 3.3.2 Breakdown Strength

The agilent semiconductor device parameter analyzer B1500A was used for the breakdown strength measurements. Figure 3.9 shows the schematic illustration of the experimental setup. For breakdown strength measurements, voltages were applied to the capacitor device using the high power source monitor unit of the B1500A device analyzer and the resulting current was monitored to detect the breakdown of the dielectric films.

# Chapter 4

# Gold Nanoparticle/SU-8 Nanocomposite

This chapter presents the enhanced dielectric properties of a photodefinable nanocomposite material containing 5 nm gold nanoparticles (NPs). The size and the dispersion of the synthesized dodecanethiol-functionalized gold NPs was characterized using transmission electron microscopy (TEM). We investigated the particle agglomeration and dispersion during the various stages of the nanocomposite synthesis using TEM. Physical properties such as dielectric permittivity, dielectric loss and breakdown strength were measured experimentally. The dependence of dielectric permittivity and loss tangent on the particle concentration and frequency was studied. The results support the use of functional metal nanoparticles for obtaining enhanced dielectric permittivity while maintaining low dielectric loss.

## 4.1 Synthesis

### 4.1.1 Dodecanethiol-functionalized Gold Nanoparticles

Gold nanoparticles were synthesized by the sodium borohydride reduction of an aqueous solution of tetrachloroauric acid in the presence of polymeric dodecylth-ioether end-functionalized poly(methacrylic acid) stabilizer, using a previously published method [100]. Next, in order to transfer the gold nanoparticles from water to an organic phase, the water-soluble polymer ligand was replaced by dodecanethiol by ligand exchange. Nanocomposite material was synthesized using the solution-mixing method.

### 4.1.2 Polymer Nanocomposite

To prepare nanocomposite suspensions, first gold nanoparticle solution and SU-8 polymer solution was prepared and then, equal amounts of the two solutions were mixed under ultrasonication. SU-8 solution was prepared by dissolving SU-8 resin in the chloroform solvent in a 1:5 ratio by weight. The concentration of the gold nanoparticle solution was adjusted by

varying the amount of the chloroform added to obtain nanocomposite suspensions with varied gold nanoparticle content. Then, nanocomposite films were prepared using drop-casting and spin-coating methods [101, 102].

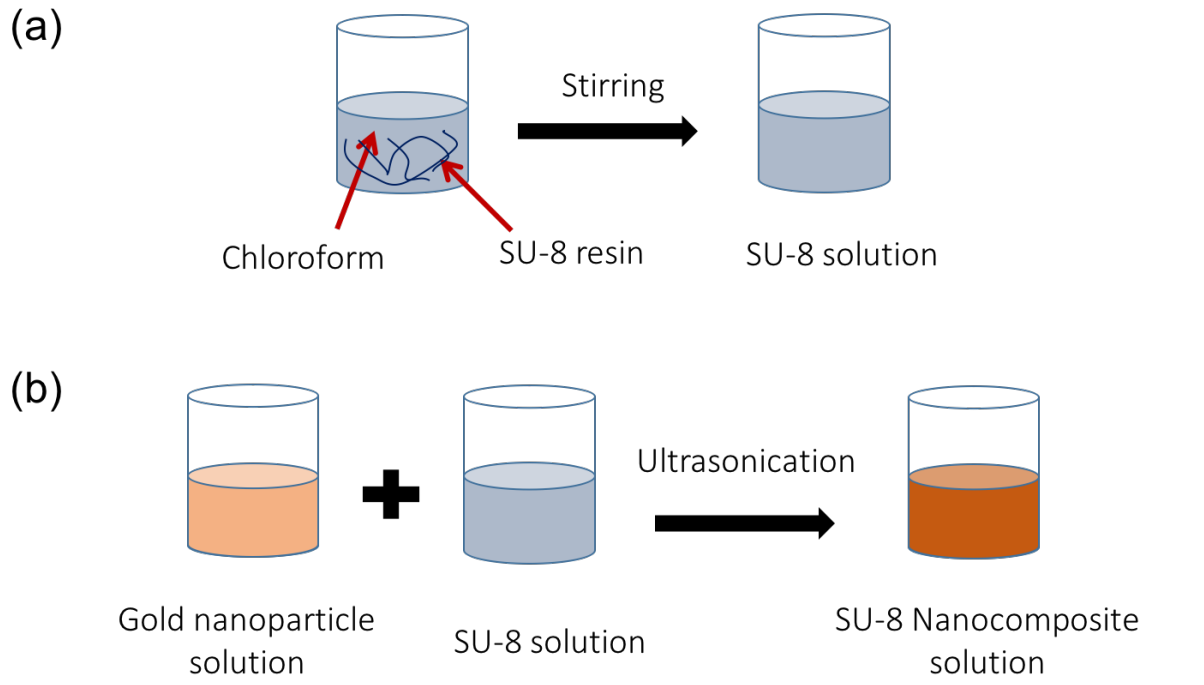


Figure 4.1: Synthesis of gold nanoparticle/SU-8 nanocomposite solution (a) polymer solution preparation, and (b) mixing of gold nanoparticle solution and polymer solution to obtain nanocomposite suspension.

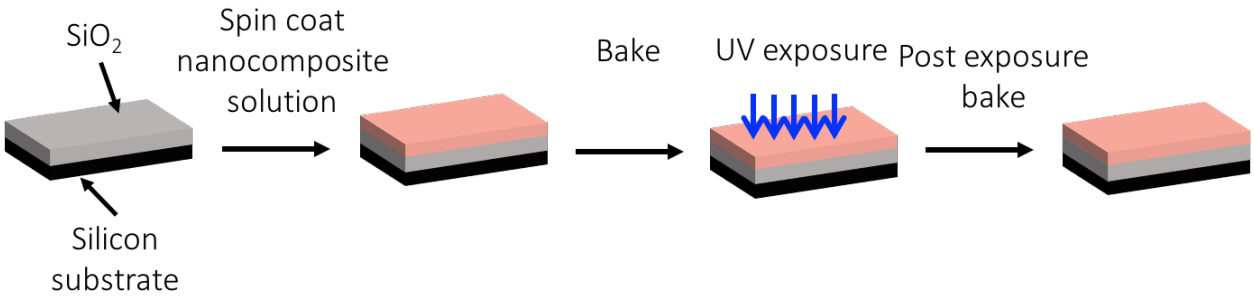


Figure 4.2: A schematic illustration of the fabrication of spin-coated nanocomposite film.

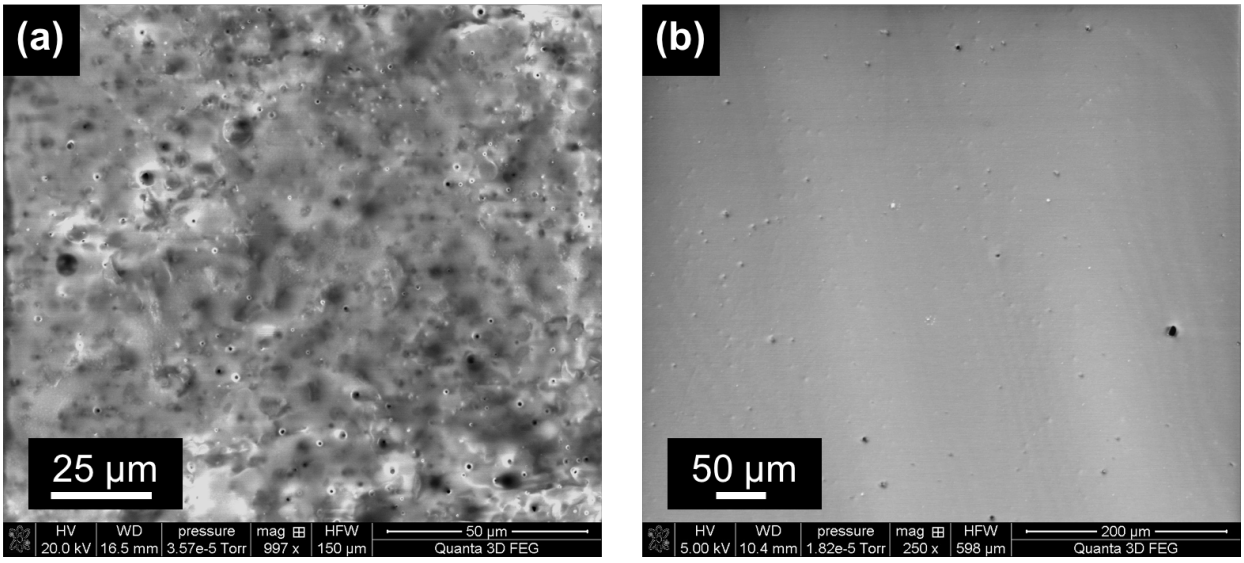


Figure 4.3: Scanning electron microscopy (SEM) image of the top surface of (a) a drop-casted, and (b) a spin-coated nanocomposite film. The drop-casted film consists of several microbubbles and voids. In contrast, the spin-coated film is uniform and has reduced number of microvoids.

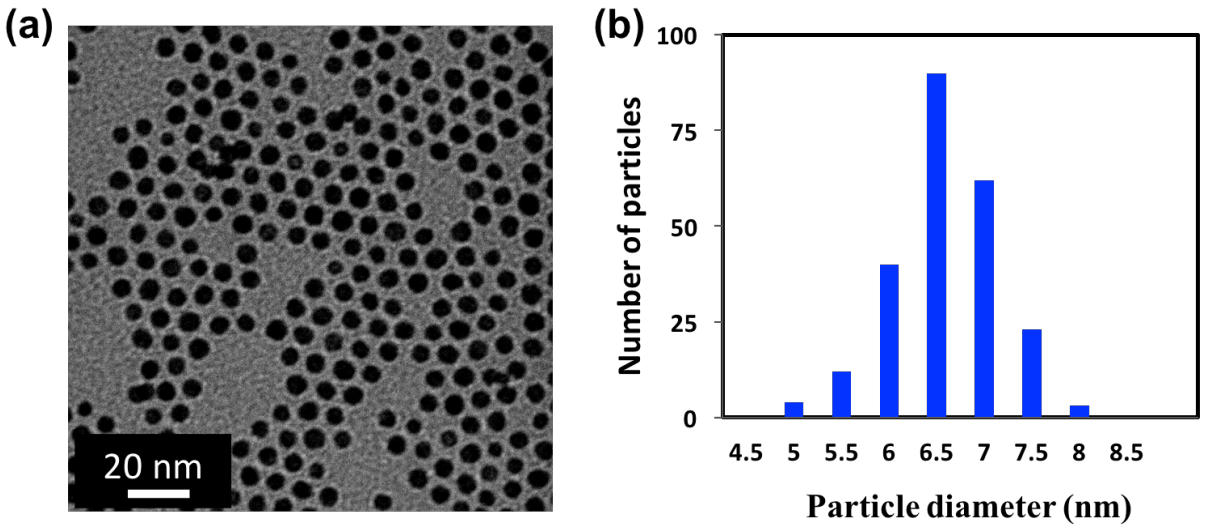


Figure 4.4: (a) TEM image of the synthesized nanoparticle solution shows that monodispersed gold nanoparticles are obtained (b) Nanoparticle size distribution.

## 4.2 Material Characterization

### 4.2.1 Nanocomposite Film Morphology

Drop-casting and spin-coating techniques were used for synthesizing the nanocomposite films. For sample-1, nanocomposite suspension was deposited onto a $SiO_2$ coated Si die by drop-casting method and dried under nitrogen environment for 24 hours. For sample-2, spin-coating method was used for casting the nanocomposite film. A 2 $\mu$m thick nanocomposite film was prepared by spin-coating followed by a bake at 95$^o$C for 5 min, UV curing and bake at 95$^o$C for 30 min to polymerize the SU-8 resin. Nanocomposite film quality and uniformity was checked using SEM.

Figure 4.3 (a) shows the SEM image (top-view) of the sample-1 nanocomposite film. Several microscale bubble and voids were observed throughout the nanocomposite film (dark regions with white periphery as seen in Figure 4.3 (a)). This might be because that cross-linking was not carried out as the sample was dried at room temperature. Figure 4.3 (b) shows the SEM image (top-view) of the spin-coated film (sample-2), a dense film is obtained with reduced voids or cracks. It is critical to minimize the number of voids and cracks as they affect the optimal performance of the nanocomposite material by increasing dielectric leakage and reducing the electric breakdown field [15]. Therefore, based on our preliminary study [102], nanocomposite films in this study were synthesized using spin-coating method rather than drop-casting.

### 4.2.2 Nanoparticle Size Distribution

To investigate the particle dispersity in the chloroform solvent, samples for the TEM analysis of gold nanoparticles were prepared. A droplet of the chloroform dispersion of gold nanoparticles was deposited onto a copper mesh grid followed by drying. Figure 4.4 (a) shows the TEM image of the nanoparticles, indicating that nanoparticles are monodispersed. It is important to characterize the particle dispersion prior to mixing them with the polymer for two reasons, one is to identify whether there is any particle agglomeration without the addition of the polymer and the other is to get an estimate of the particle size. The absorption spectra of the gold nanoparticles with different concentrations are shown in Figure 4.5 (red curve: as-synthesized nanoparticle dispersion in chloroform; blue curve: nanoparticle solution after 2 times dilution). At a constant particle size, the optical absorbance was linearly related to the concentration of gold nanoparticle solution, which is in accordance with the Beer-Lambert law of absorbance showing a linear relationship between the absorbance and the concentration of an absorber [103].

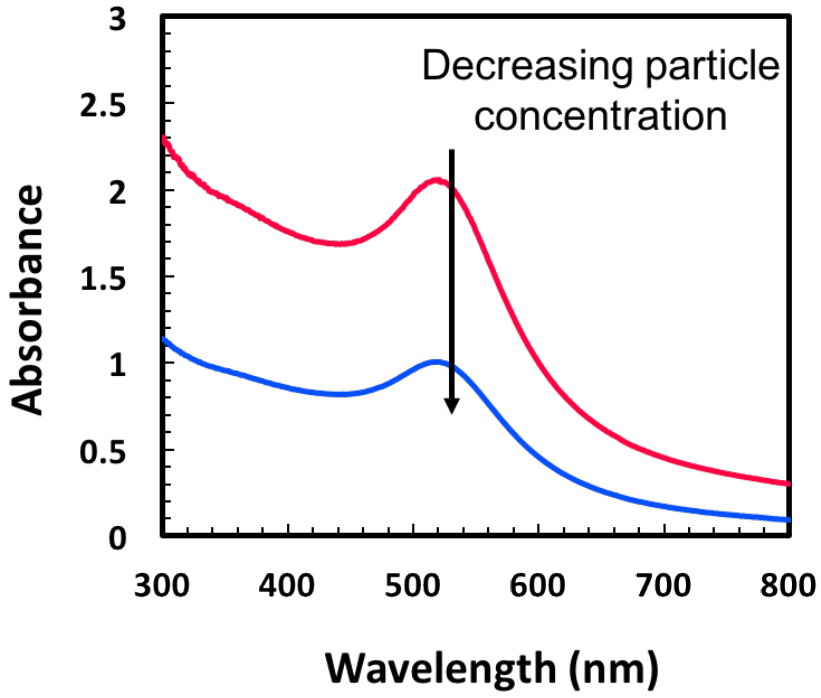


Figure 4.5: The absorption spectra shows the variation of the absorbance with the gold particle concentration at a fixed particle size.

### 4.2.3 Nanoparticle Dispersion in Gold Nanoparticle/SU-8 Polymer

We studied the particle agglomeration and dispersion in the SU-8 polymer by characterizing the nanocomposite films using TEM. To characterize the nanoparticle dispersion in the gold nanoparticle/SU-8 polymer composite material, thin slices (50-80 nm) of the cross-section of the nanocomposite film were prepared by Reichert ultramicrotome for TEM imaging. The nanocomposite sample was cut with a diamond knife attached to a boat in which the cut thin slices float on top of water. A few of these slices were collected and placed onto the TEM grid for imaging. Figure 4.6 (a) shows a TEM image of the cross-section of the overall nanocomposite film containing 5% w/w nanoparticle content. The film is resting on an epoxy substrate. During microtoming, due to the shear-induced distortions, the nanocomposite film cross-section was distorted, therefore resulting in a cross-section with non-uniform (uneven) thickness as seen in Figure 4.6 (a). To observe nanoparticle dispersion, images were captured in higher magnifications from different areas of this nanocomposite film as shown in Figure 4.6 (b-d). It can be observed that some portion of the gold nanoparticles have agglomerated into clusters of size 20-25 nm in diameter, but the overall distribution of nanoparticles/nanoclusters is homogeneous throughout the nanocomposite film.

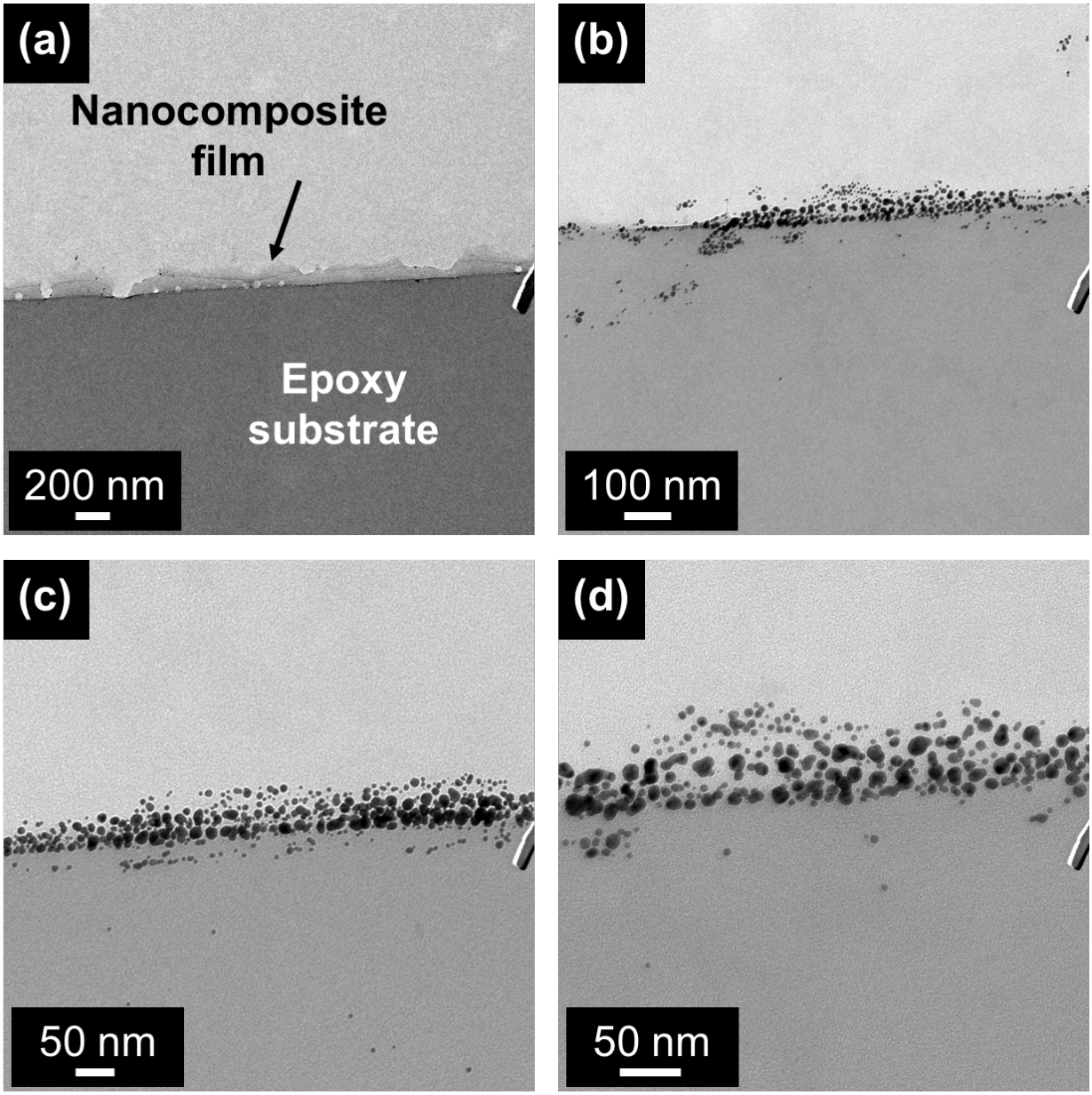


Figure 4.6: TEM images of the spin-coated nanocomposite film containing a gold nanoparticle concentration of 5% w/w. (a) Cross-sectional view of overall nanocomposite film and (b-d) zoomed-in view of nanoparticles in SU-8 matrix at different magnifications.

## 4.3 Electrical Characterization

To characterize the dielectric properties, electrical measurements were performed using the probe station (Signatone, model H100) with a blunt tungsten probe tip to minimize the

mechanical damage on the soft organic nanocomposite films. Characterization of both nanocomposite and SU-8 only capacitor devices was done in an ambient atmosphere. Capacitance measurements were made using the multi-frequency capacitance measurement unit (MFCMU) of the B1500A semiconductor parameter analyzer.

### 4.3.1 Capacitor Device Design and Fabrication

Parallel plate-type capacitor devices were fabricated to measure the dielectric properties of the gold nanoparticle/SU-8 nanocomposite material. In short, as a first step, $SiO_2$ (100 nm thick) was deposited on a silicon (Si) substrate (size of 10 mm $\times$ 20 mm). For the bottom electrode of the capacitor, aluminum (200 nm thick) was deposited using sputtering machine, followed by the spin-coating of nanocomposite film. For the top electrodes, gold metal (100 nm thick and 2 mm diameter) was directly deposited onto the nanocomposite film. Figure 4.7 shows the schematic of the capacitor device fabricated in a metal-insulator-metal configuration. The thickness of each film was recorded using a stylus contact profilometer (Alpha-Step IQ Surface Profiler).

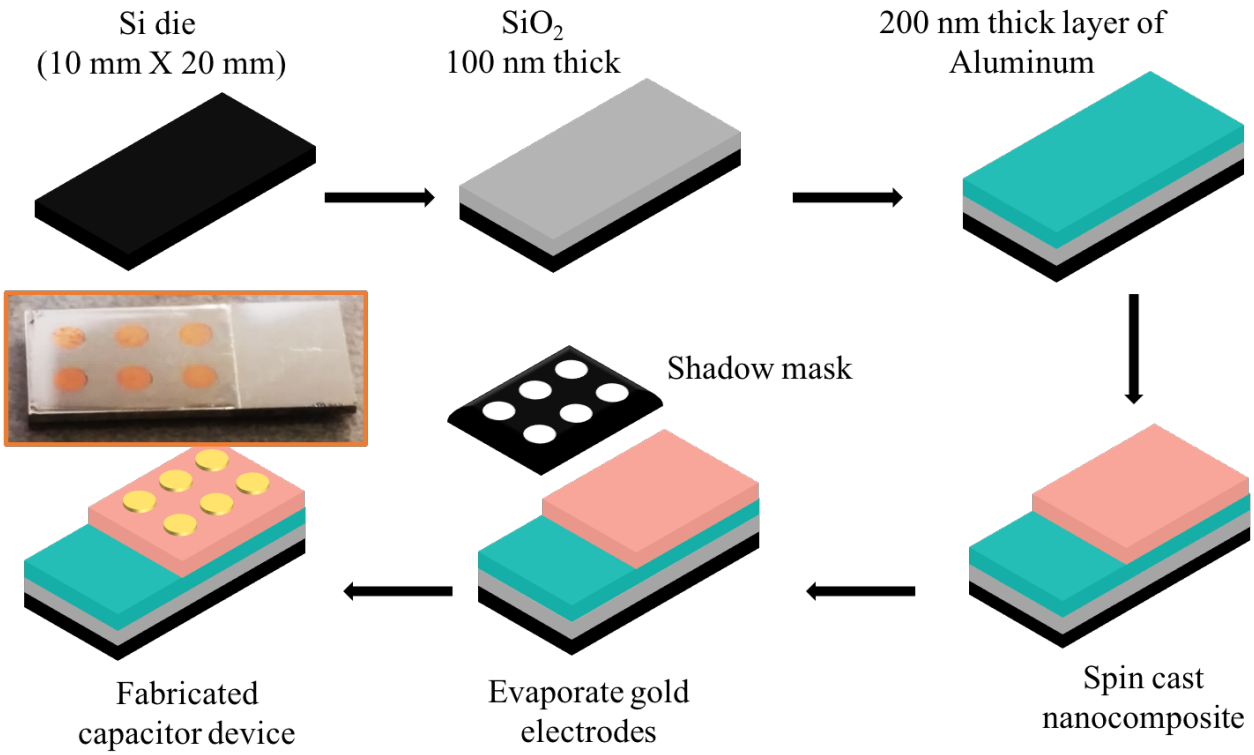


Figure 4.7: Fabrication procedure of the capacitor device on a silicon substrate.

### 4.3.2 Dielectric Properties of Gold Nanoparticle/SU-8 Nanocomposite

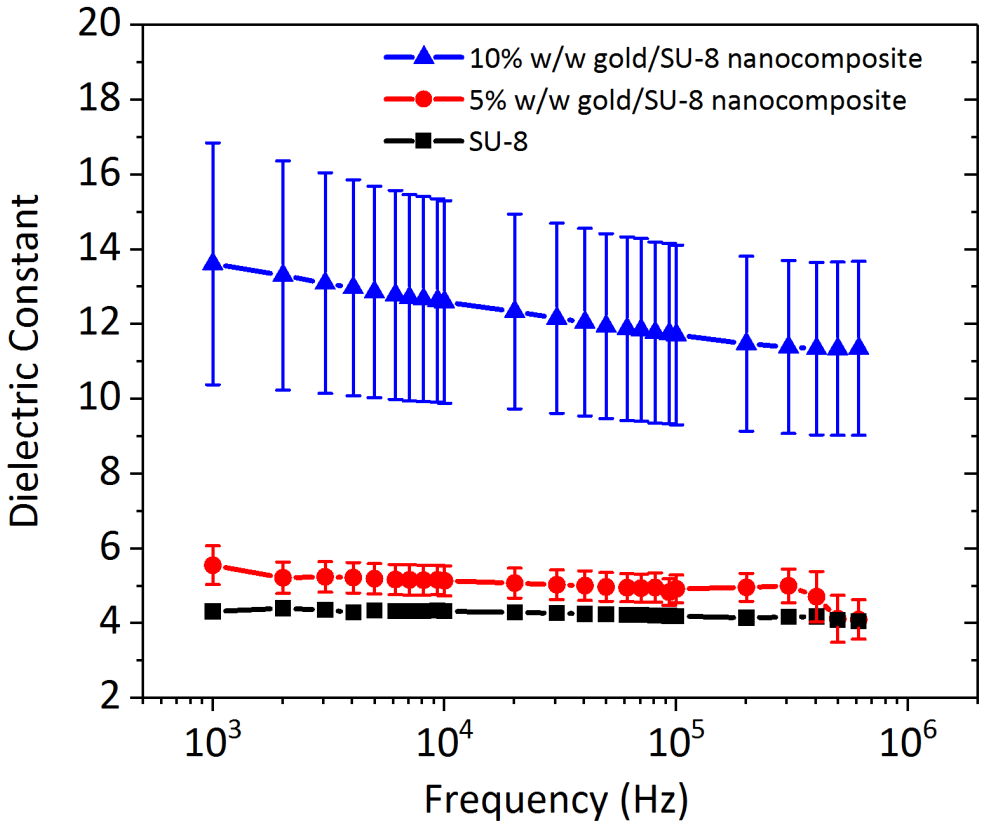


Figure 4.8: Frequency dependence of dielectric constant of the gold nanoparticle/SU-8 nanocomposite films. The nanocomposite samples have higher dielectric constant than the polymer only samples in the whole frequency range.

In Figure 4.8, average dielectric constant values were plotted against frequency for nanocomposite films with varied nanoparticle concentration. The error bars in Figure 4.8 represent one standard deviation of the mean dielectric constant. Figure 4.8 shows that the gold/SU-8 nanocomposite samples films have higher dielectric constant than the polymer only (i.e., SU-8 without gold nanoparticles) samples in the whole frequency range. An average dielectric constant of 13.6 at 1 kHz was observed for 10% w/w nanocomposite samples. The increase in the dielectric constant of nanocomposite is because of the accumulation of charges at the particle-polymer interface resulting from the interfacial polarization. For nanocomposite films, the dielectric constant decreased at high frequency values due to the loss of the contribution of the interfacial polarization mechanism to the total polarization. At high frequencies, the electric field oscillates faster than charges that can accumulate at the particle-polymer interface, reducing the dielectric permittivity [104]. This behavior becomes

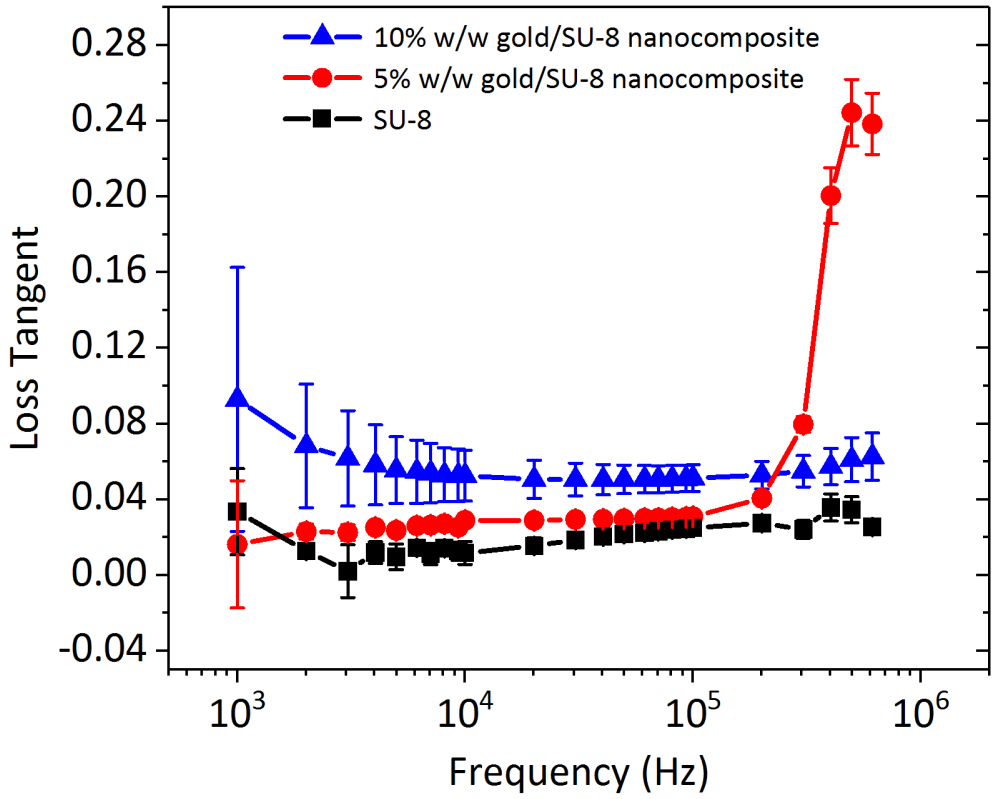


Figure 4.9: Loss tangent of the gold nanoparticle/SU-8 nanocomposite films with varied nanoparticle concentration. The average loss tangent value for nanocomposite capacitors is slightly greater than the SU-8 only samples. This is due to the presence of particle agglomerates in the SU-8 matrix for nanocomposite capacitors having 10 wt% particle content.

noticeable in the case of the nanocomposite films containing a nanoparticle concentration of 10% w/w. The dielectric constant values are expected to increase with further increase in particle concentration. However, we did not measure the dielectric properties beyond 10% w/w nanoparticle concentration due to the increase in nanoparticle agglomeration in the nanocomposite films. For nanocomposite film containing 5% w/w gold nanoparticles, the error bars are relatively small, implying that the nanoparticle distribution is homogeneous. This is in agreement with the TEM data shown in Figure 4.6. However, for 10% w/w nanocomposite films, variation from the mean dielectric constant and loss tangent is relatively large as depicted by the large error bars in Figure 4.8. This implicitly suggests an inhomogeneous nanoparticle distribution in nanocomposite films containing 10% w/w gold nanoparticles.

Figure 4.9 shows the loss tangent values for the nanocomposite and SU-8 only capacitors, with the error bars showing one standard deviation of the mean loss tangent. It can be observed that the average loss tangent for nanocomposite capacitors is higher than the SU-

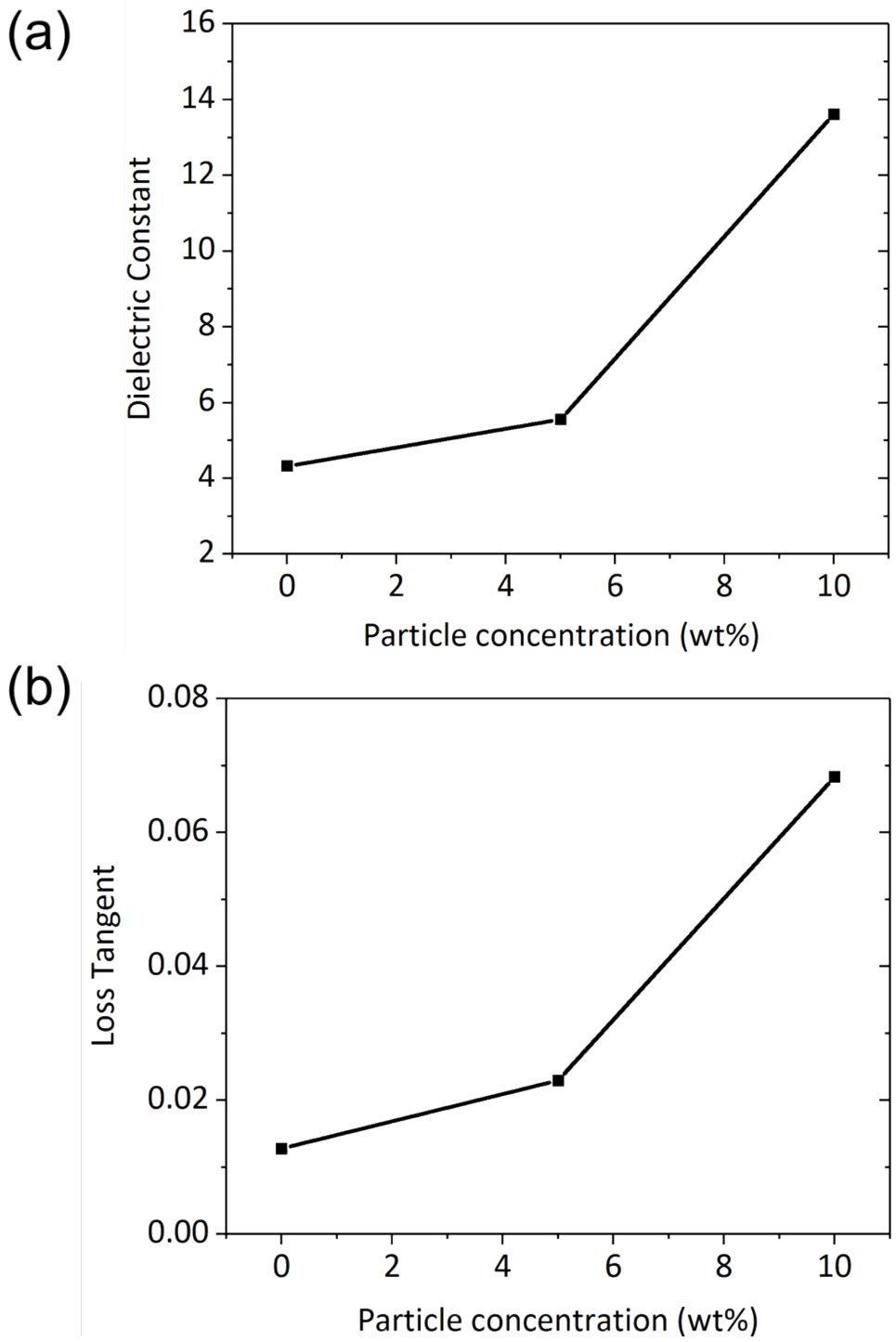


Figure 4.10: Variation of (a) dielectric constant and (b) loss tangent with nanoparticle concentration for gold nanoparticle/SU-8 nanocomposite films at 1 kHz.

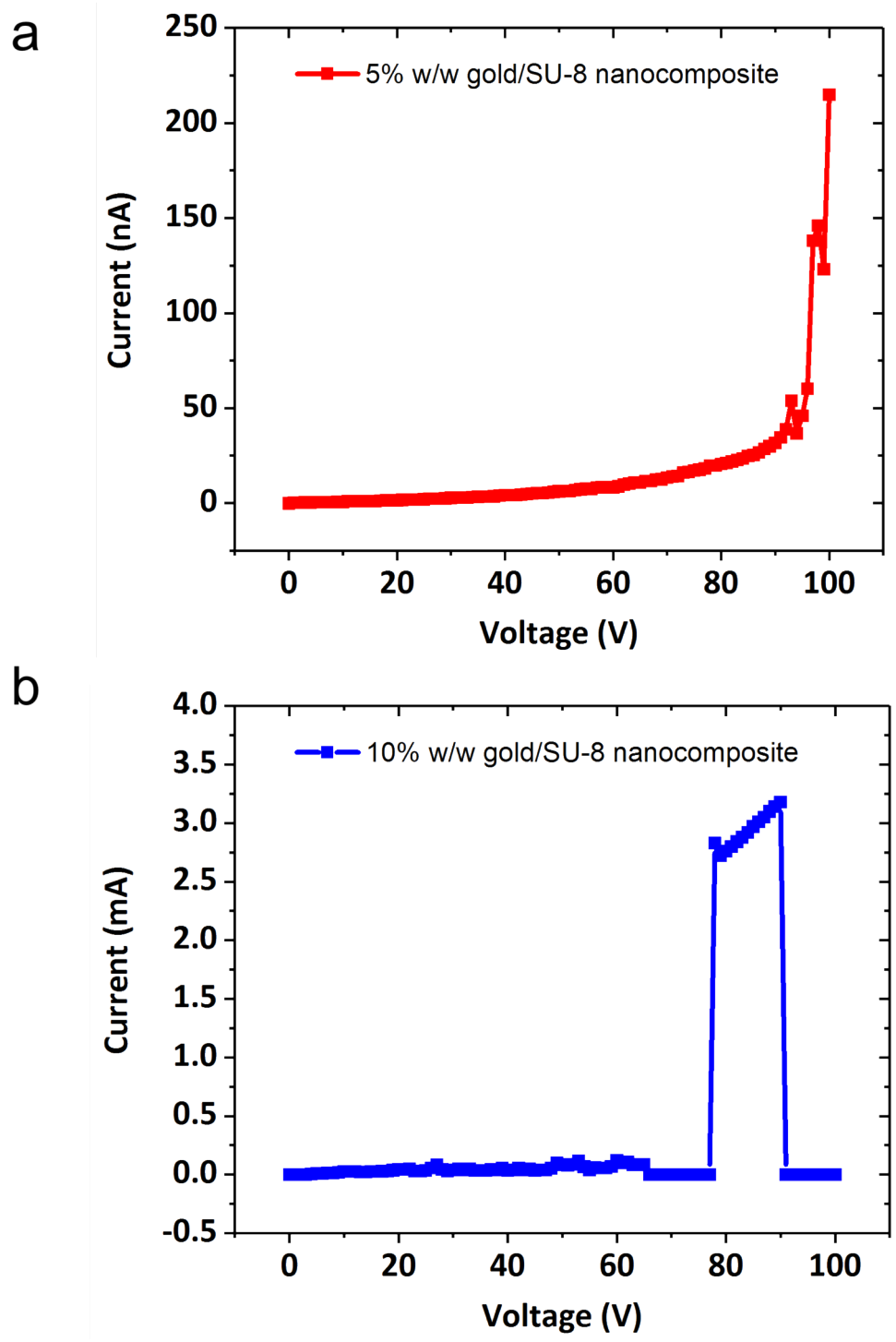


Figure 4.11: Breakdown strength measurement of 5% and 10% w/w gold nanoparticle/SU-8 nanocomposite films. The sharp rise in current at $\sim$ 97 and $\sim$ 78 V indicate the breakdown for 5% and 10% w/w nanocomposite films respectively.

8 only capacitors. This is expected due to the presence of particle agglomerates in the SU-8 matrix for nanocomposite capacitors (see Figure 4.6). However, the observed loss tangent values are relatively low in comparison to the previously published values [105]. In addition, the dielectric loss of the nanocomposite films showed weak frequency dependence at high frequency ranges ($>$ 10 kHz). Figure 4.10 (a) shows the effect of the nanoparticle concentration on the dielectric properties of gold nanoparticle/SU-8 nanocomposite measured at 1 kHz. The enhancement in the dielectric permittivity increased rapidly when the particle concentration is higher than 5% w/w. A dielectric permittivity of 13.6 was observed at a 10% w/w particle content. The effect of particle concentration on loss tangent is illustrated in Figure 4.10 (b). The dielectric loss increased with the increase in the particle concentration. However, the measured dielectric loss values are still quite low. For example, the loss tangent was measured to be $\sim$ 0.07 for 10% w/w nanocomposites. Although further parametric studies including the change of ligands and base polymer, spin-coating speed, baking time and temperature can be leveraged to improve the particle dispersion at high nanoparticle concentrations, the enhanced dielectric properties of photodefinable nanocomposites were achieved using a combination of ligand-modified gold nanoparticles and SU-8 polymer.

### 4.3.3 Breakdown Strength Measurement of Gold Nanoparticle/SU-8 Nanocomposites

Tests were performed by applying a voltage between the top (gold) and bottom (aluminum) electrodes. The breakdown strength was measured using the voltage ramp test procedure, where the voltage was linearly increased until the breakdown occured. The current starts at a low value and ramps exponentially until the dielectric breakdown. A breakdown was evident under three scenarios; a sharp rise in the current, a visually noticeable damage in the dielectric film, or an audible sound.

The current-voltage characteristics of the gold nanoparticle/SU-8 nanocomposite films are shown in Figure 4.11. For 5% w/w nanocomposite films, at a low voltage of 10 V, the measured current was $\sim$ 1 nanoamperes (nA). A spike in the current was observed at 97 V indicating the breakdown of the dielectric film as shown in Figure 4.11 (a). The breakdown behavior of the 10% w/w nanocomposite film is shown in Figure 4.11 (b). The current rose sharply to 2.8 milliamperes (mA) at 78 V suggesting the film breakdown. The average breakdown strength for the 5% and 10% w/w gold nanoparticle/SU-8 nanocomposite films was measured to be 97 and 70 MV/m respectively.

## 4.4 Discussion

In summary, a photodefinable nanocomposite with enhanced dielectric properties is successfully developed using 5 nm dodecanethiol-functionalized gold nanoparticles and SU-8 polymer. The dispersion of the gold nanoparticles in the SU-8 polymer was investigated using electron microscopic analysis. The nanocomposite films show relatively low dielectric

loss and considerably high dielectric constant. At a particle concentration of 10% w/w, nanocomposite films exhibited an average dielectric constant of 13.6 and loss tangent of 0.09 at 1 kHz.

# Chapter 5

# Gold Nanoparticle/PVDF Nanocomposite

This chapter reports on the design and development of a nanocomposite dielectric developed by embedding PVP-encapsulated gold nanoparticles in the PVDF polymer matrix. The coating material is carefully tailored so as to aid in the dispersion of gold nanoparticles while providing local electrical resistance to allow increased volume fractions of particles in the polymer scaffold. The surface functionalization of gold nanoparticles with PVP facilitates favorable interaction between the particle and polymer phase, enhancing nanoparticle dispersion. Since PVP is miscible with PVDF, the particle dispersion is enthalpically favored. Furthermore, PVDF has high breakdown strength (>700 MV/m) [106] and the overall dielectric permittivity of nanocomposites can be increased owing to nanoscale conductive fillers [19, 20], thus, serving as a high energy density dielectric material and providing several potential applications. To study the effect of entropic interactions on particle dispersion, nanocomposites with two different particle sizes (5 and 20 nm in diameter) were synthesized and characterized. A uniform particle distribution was observed for nanocomposite films consisting of 5 nm gold particles, in contrast to the film with 20 nm particles. The frequency-dependent dielectric permittivity and the loss tangent were measured for the nanocomposite films. Moreover, the dielectric breakdown strength measurements were done on the nanocomposite films.

The first section of this chapter discusses the effect of process conditions such as film-casting method and the processing temperature on the development of nanocomposite films with lesser number of voids. The next sections of this chapter discuss the particle dispersion in the PVDF polymer for 5 nm and 20 nm gold nanoparticles. The last section of this chapter covers the dielectric permittivity and breakdown field strength properties of the nanocomposite material.

## 5.1 Nanocomposite Synthesis and Material Characterization

To identify the appropriate processing conditions for the synthesis of nanocomposite films, first control samples were prepared using PVDF. A 10% w/w polymer solution was prepared by mixing PVDF in form of pellets with the DMF solvent, followed by heating at 100$^o$C continuous stirring, until entire amount of PVDF was dissolved. Sample-1 was prepared by drop-casting the as synthesized polymer solution film onto a $SiO_2$ substrate, followed by annealing in a vacuum oven at 50$^o$C for 24 hours. Another sample was prepared by spin-coating the PVDF solution at 1500 rpm, 30 sec and annealing at 100$^o$C for 2 hours.

The morphology of the resulting polymer films was studied using SEM. It can be observed in Figure 5.1 (a) that the drop cast film is porous, and has loosely connected PVDF spherulites. This could be attributed to the diffusion of ambient water molecules into the liquid composition solution, because water is miscible with DMF. However, PVDF is not soluble in water, so phase separation might have occurred. Spin-coating was also used for synthesizing the nanocomposite film. Fig. 5.1 (b) is the SEM image of the top surface of the spin coated film. In comparison to the drop-cast film, it can be observed that a dense film is achieved with no voids. This could be due to the faster evaporation of the solvent in case of the spin coated film and hence, less time available for water molecules to diffuse in the wet film.

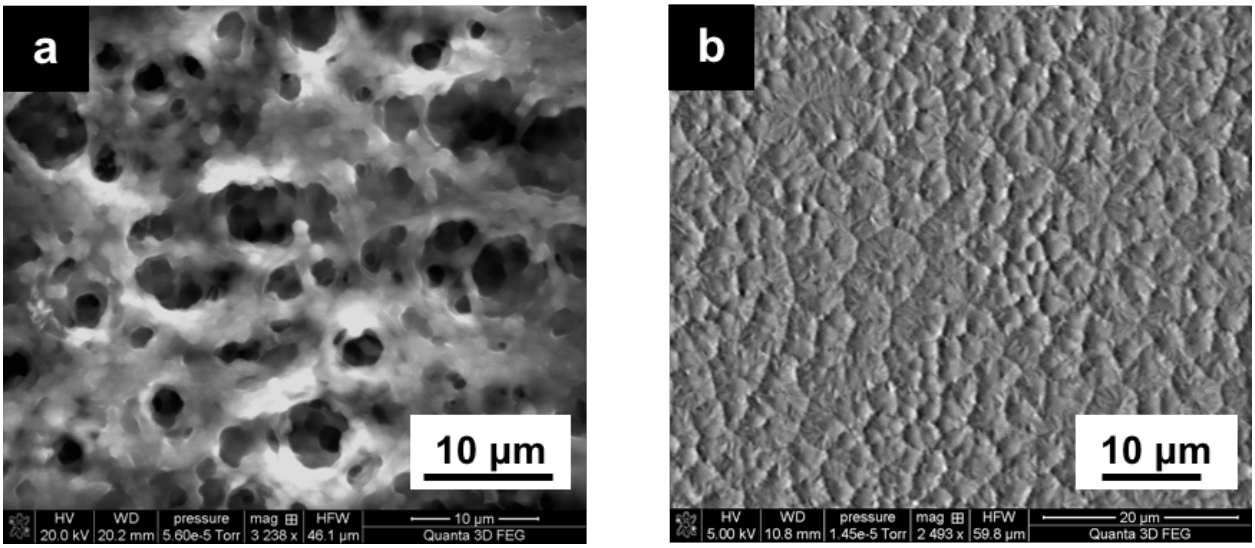


Figure 5.1: SEM image of (a) drop-casted and (b) spin-coated PVDF polymer film. Drop-casted film exhibits porosity as evident from the voids throughout the film, whereas no voids were observed in the spin-coated film.

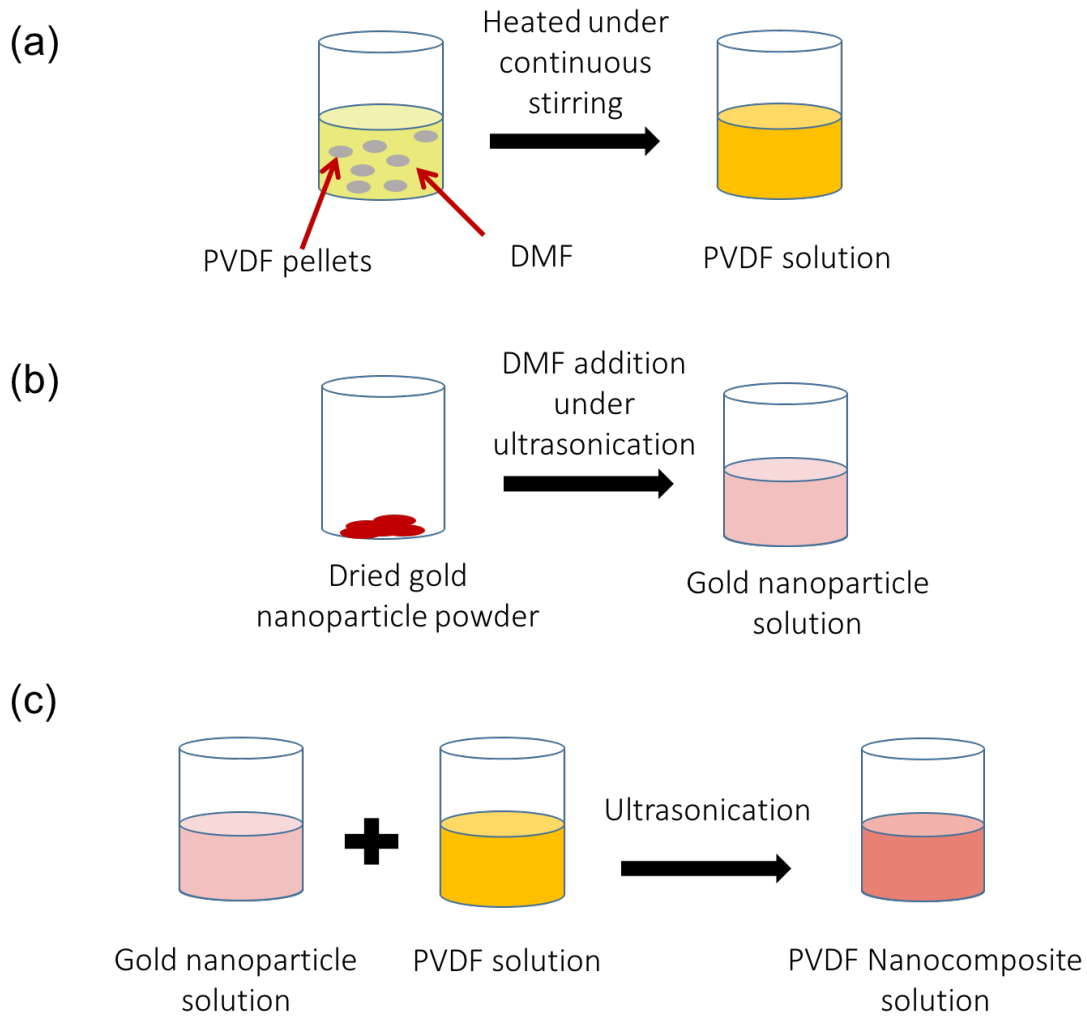


Figure 5.2: Synthesis of PVDF nanocomposite solution (a) polymer solution preparation, (b) preparation of the gold nanoparticle dispersion, and (c) mixing of gold nanoparticle solution and polymer solution to obtain the nanocomposite suspension.

The morphology of the gold nanoparticle (5 nm)/PVDF nanocomposite films was investigated as well. In order to fabricate nanocomposite films, a nanocomposite suspension (1 % w/w nanoparticle content) was prepared by directly mixing the particle suspension with polymer solution under sonication for an hour at room temperature as shown in Figure 5.2. PVDF nanocomposite films were spin-coated (Figure 5.3) under the same process conditions as described earlier for PVDF films. Figure 5.4 (a) and (b) show the surface morphologies of the drop-casted and spin-coated nanocomposite films. It is evident that a similar behavior was observed in the case of the nanocomposite films.

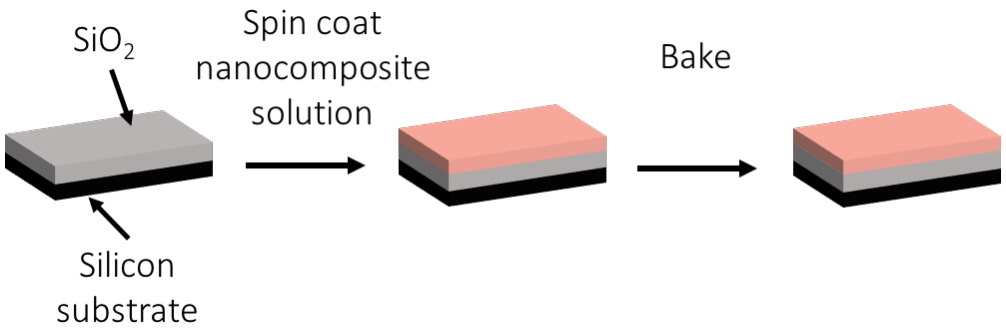


Figure 5.3: A schematic illustration of the fabrication of spin-coated PVDF nanocomposite film.

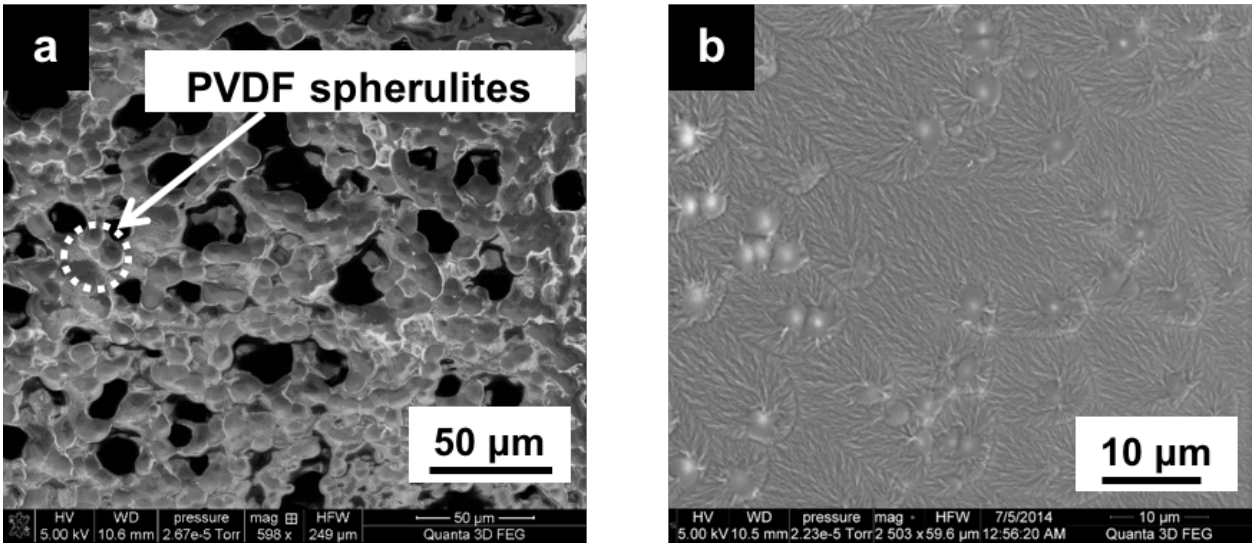


Figure 5.4: SEM image of (a) drop-casted and (b) spin-coated gold nanoparticle (5 nm)/PVDF polymer composite film.

### 5.1.1 Grazing Incidence X-ray Diffraction

Grazing-incidence wide-angle scattering (GIWAXD) was used to characterize the different phases of the PVDF polymer. The crystal structures of PVDF, 1% and 12.5% w/w gold (5 nm)/PVDF films annealed at 100°C, were characterized by GIWAXD as presented in Figure 5.5. For pure PVDF films, the less intensive peaks at $18.6^o$ and $20.1^o$ attribute to $(020)\alpha$ and $(110)\alpha$ crystal planes respectively [107].

A broad peak centered at $21.4^o$ is also observed, it could be explained as (012) $\gamma$-prohibited [108]. WAXD pattern of 1% w/w PVDF nanocomposite shows a broad peak centered at $21.4^o$, its full width at half maximum ranges from $20.6^o$ to $23^o$. It is attributed

to the (110) and (200) crystal planes of the $\beta$ phase, [107] although contributions from the $\gamma$ phase cannot be excluded. The peak at $21.4^o$ is typical for the $\gamma$ phase, and it could be explained as (012) $\gamma$-prohibited [108]. Similar to the 1% case, the WAXD pattern of 12.5% w/w PVDF nanocomposite shows an intense broad peak around $20.6^o$ that corresponds to the (110) and (200) crystal planes of the $\beta$ phase [107]. The broad peak centered at $26.5^o$ can be attributed to either the $\alpha$ or the $\gamma$ phase [108]. For PVDF, and nanocomposite films with 1 and 12.5% w/w, a peak is observed at $16.5^o$ that cannot be explained by any of the known crystal structures of PVDF.

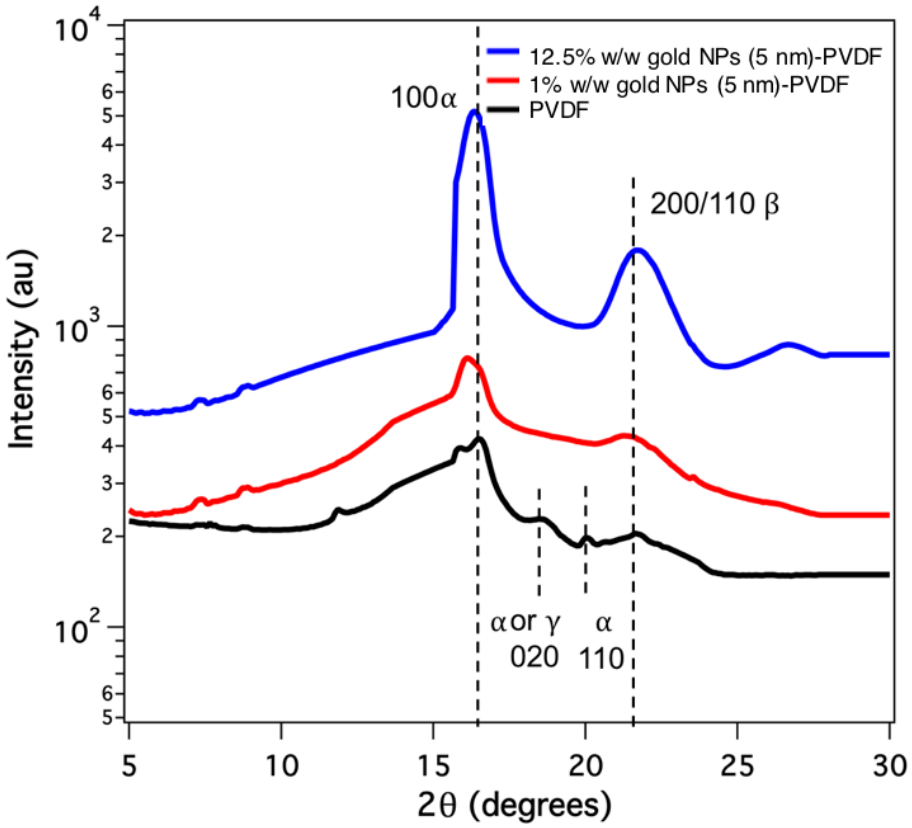


Figure 5.5: GIWAXD patterns obtained for (a) PVDF film, gold (5 nm)/PVDF nanocomposite with (b) 1% and (c) 12.5% w/w nanoparticle content.

### 5.1.2 Nanoparticle Dispersion in PVDF

TEM was used to check nanoparticle size and agglomeration after preparing the nanoparticle solution. Figure 5.6 shows that nanoparticles are monodispersed, and hence, no particle agglomeration occurred during the nanoparticle solution preparation. Particle size is estimated to be $4.40 \pm 0.53$ nm using the ImageJ software.

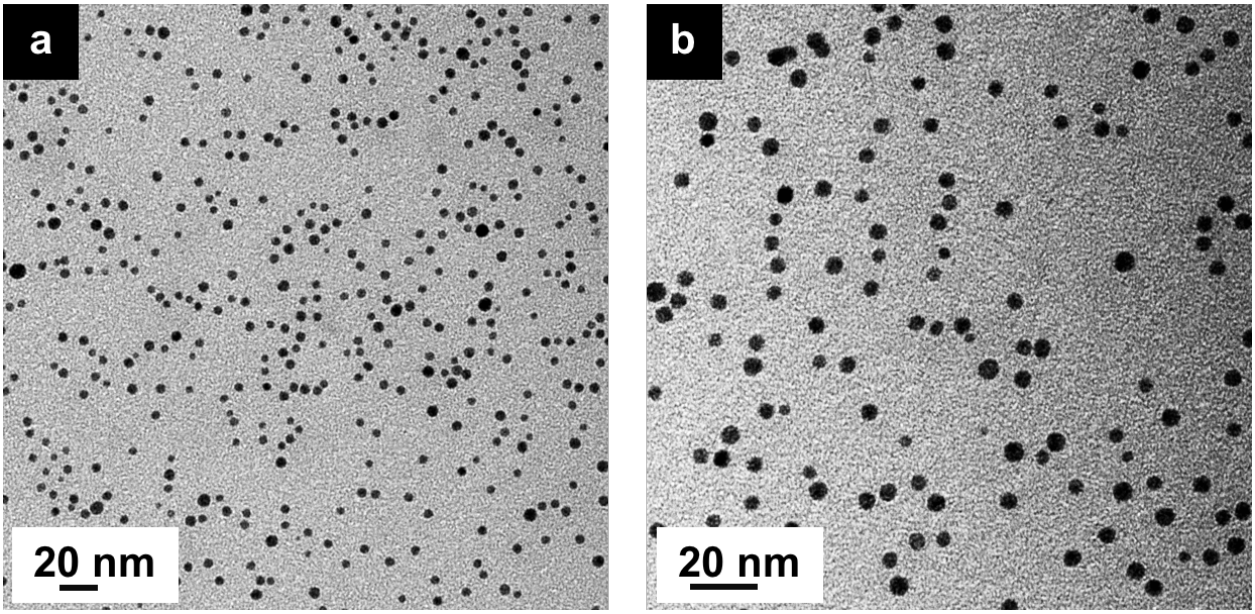


Figure 5.6: TEM analysis of PVP-grafted 5 nm gold nanoparticles. It was observed that nanoparticles were monodispersed.

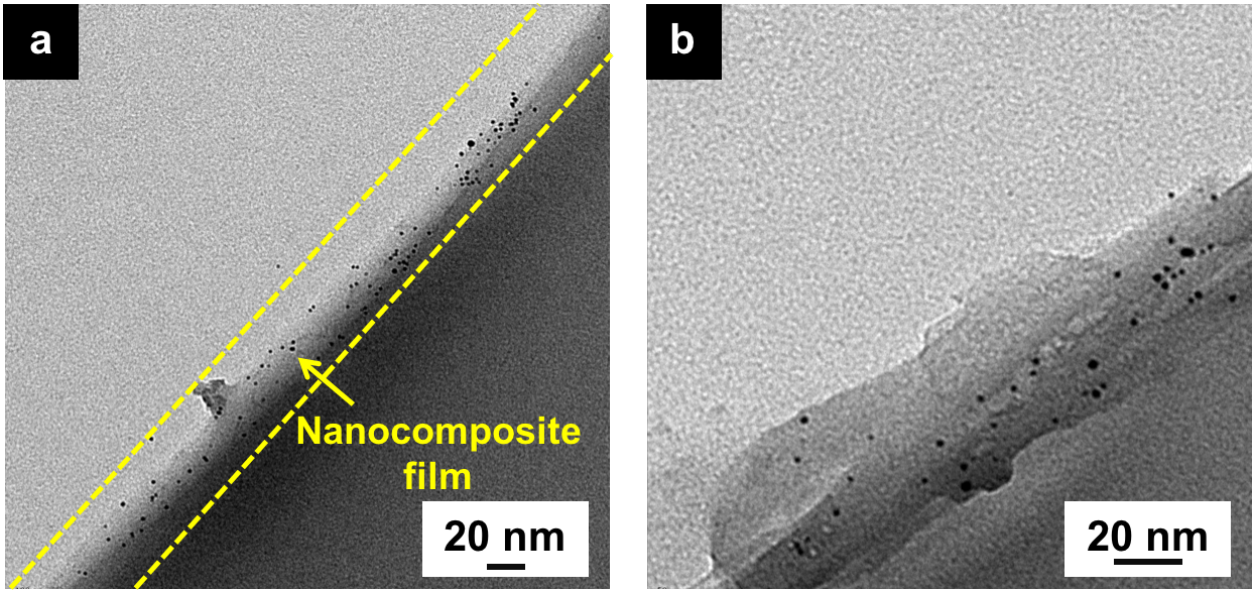


Figure 5.7: TEM image of cross-section of nanocomposite film with gold nanoparticle concentration of 1% w/w. TEM images qualitatively suggests that a uniform dispersion of gold nanoparticles in PVDF has been achieved.

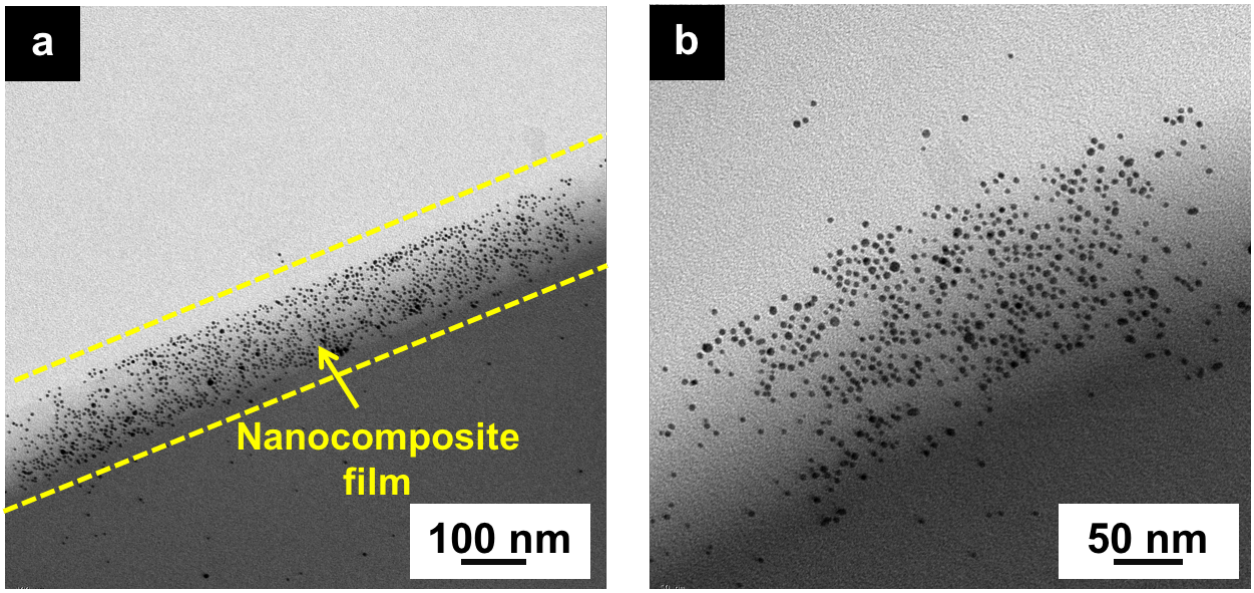


Figure 5.8: Gold nanoparticle/PVDF polymer composite film with 5% w/w nanoparticle content at different magnification levels (a) and (b).

The spatial distribution and the dispersity of the gold nanoparticles in the PVDF polymer matrix was studied using TEM [109, 110]. Nanocomposite film cross-sections ($40 - 80$ nm thick) were obtained using a Reichert microtome. Figure 5.7 shows the cross-section of the nanocomposite film with fairly low nanoparticle content (1% w/w) in different magnifications. The nanoparticles appear to be monodispersed i.e. no particle agglomeration is observed in the nanocomposite film.

To study the effect of the increase in particle concentration on the distribution of nanoparticles, TEM analysis was performed for nanocomposite films with increased nanoparticle concentration. A nanocomposite film with 5% w/w of nanoparticles is shown in Figure 5.8. Figure 5.8 (b) shows a high magnification view of the 5% w/w nanocomposite film. No dominant aggregation of the gold nanoparticles at the air/film interface is observed. These images qualitatively indicate that a uniform dispersion of nanoparticles with no agglomeration has been achieved. The particle distribution suggests that the gold nanoparticles are effectively insulated by the polymer. Since nanoparticle agglomeration results in high dielectric loss and reduced electrical breakdown strength, a uniform particle distribution with no agglomeration is imperative to obtain optimal enhancement in the dielectric properties.

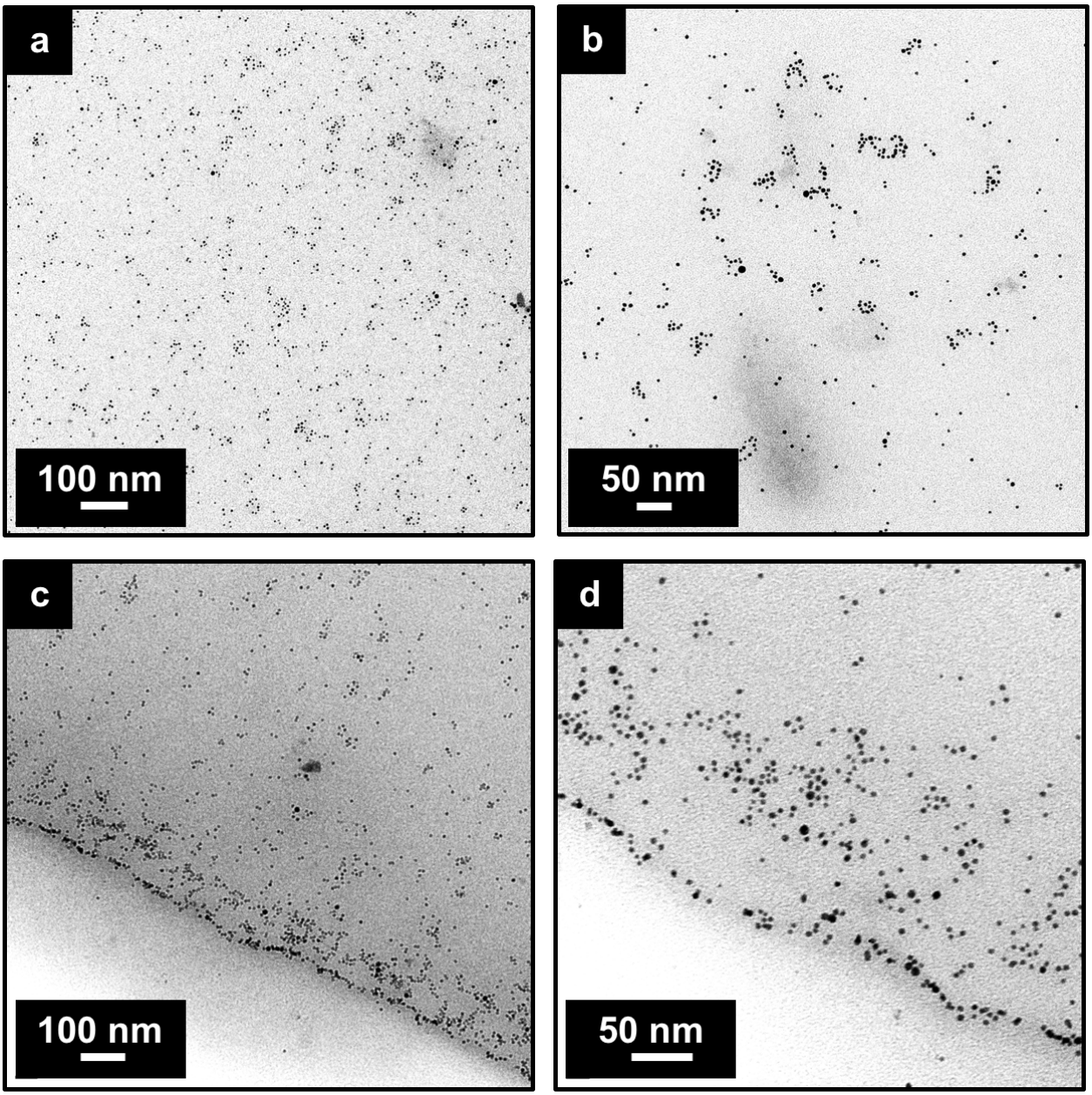


Figure 5.9: Gold nanoparticle/PVDF polymer composite film with 12.5% w/w nanoparticle content at different magnifications. Images a and b are taken from the bulk of the polymer, and images c and d are captured near the air/film interface region.

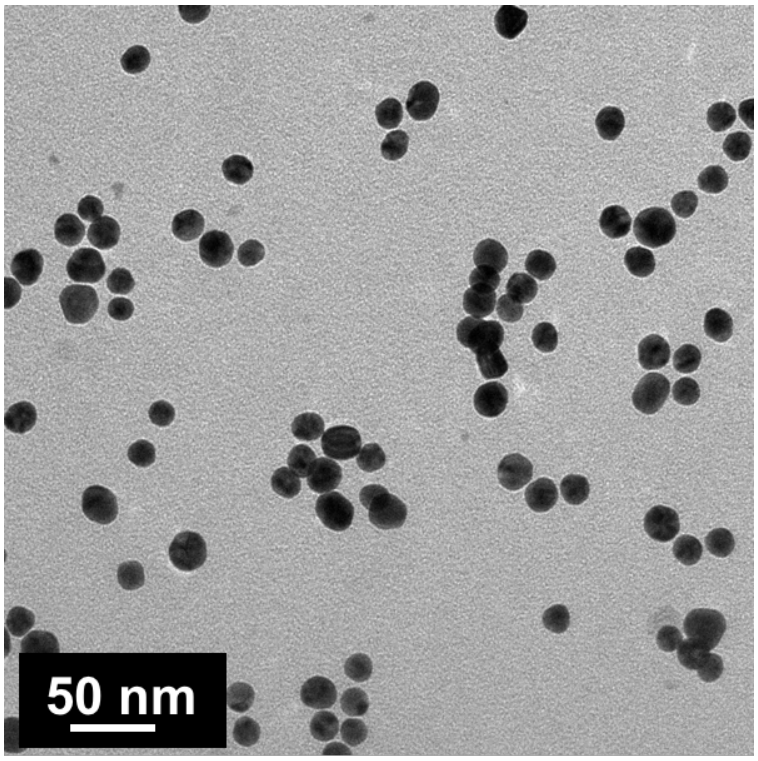


Figure 5.10: TEM image of PVP-coated 20 nm gold nanoparticles.

Gold nanoparticle distribution in the nanocomposite film with 12.5% w/w particle content is illustrated in 5.9. Electron micrographs are captured from the different regions of the nanocomposite film. Figures 5.9 (a), (b) represent the distribution of the nanoparticles in the interior regions i.e. away from the air/film and film/substrate interface. It can be concluded that the particles are uniformly distributed in the PVDF matrix and no dominant segregation of the gold nanoparticles is observed. Figure 5.9(c) shows the particle dispersion in the nanocomposite film near the air/film interface. The TEM image suggests that the relative concentration of nanoparticles near the air/film interface is higher than in the interior regions of the nanocomposite film. Although the uniform distribution of nanoparticles is desirable throughout the nanocomposite film (even near the air/film interface), a magnified view in Figure 5.9(d) shows that the gold nanoparticles are well-dispersed in the PVDF polymer matrix with no agglomeration. It is noteworthy that single gold particles are embedded in the PVDF polymer matrix, with an average size of 5 nm. Typically, nanoparticle addition in polymer leads to particle agglomeration, which is undesirable for energy storage because agglomerates can form percolation pathways for current leakage, resulting in increased energy loss.

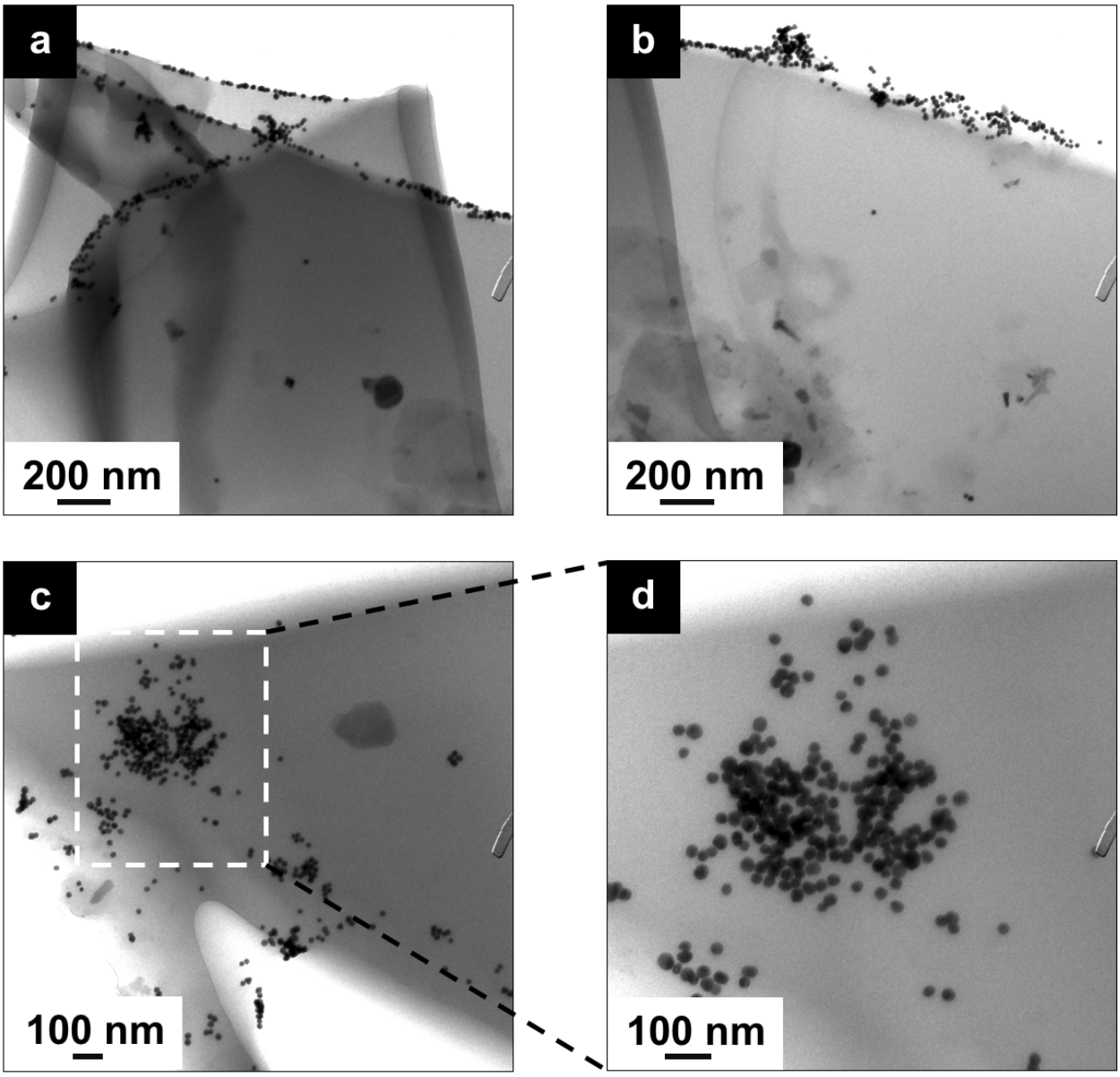


Figure 5.11: TEM images of nanocomposite film containing 20 nm gold nanoparticles (5 % w/w). Images (a) and (b) show that nanoparticles are excluded from the host polymer matrix to the air/film interface, with fewer particles embedded in the polymer matrix as shown in image (c). A high-magnification view of the area highlighted by the white box in image (c) is shown in image (d).

To study the effect of nanoparticle size on particle dispersity in the polymer composite, nanocomposite films embedded with 20 nm PVP-functionalized gold nanoparticles were synthesized and characterized. TEM micrograph of 20 nm gold nanoparticles is shown in Figure 5.10. It shows that the nanoparticles are monodispersed. To study the spatial dispersion and agglomeration of gold nanoparticles in the PVDF polymer matrix, nanocomposite films containing 5% w/w of gold (20 nm) nanoparticles were prepared under the same process conditions as used for 5 nm gold nanoparticle/PVDF nanocomposite films. Figure 5.11 show the electron micrographs of a gold (20 nm)/PVDF nanocomposite film having a particle concentration of 5% w/w. TEM images are captured from the various regions of the nanocomposite film. Figure 5.11 (a), (b) shows that the nanoparticles are being expelled from the bulk of the polymer toward the air/film interface. Certain regions of the film have nanoparticles embedded in the polymer, as shown in Figure 5.11 (c). However, the particle dispersion is not uniform. Figure 5.11 (d) shows a high magnification electron micrograph of the region marked by the white box in Figure 5.11 (c). From the TEM analysis, it can be concluded that the distribution of 20 nm gold nanoparticles in the PVDF host matrix is inhomogeneous. This is in contrast to the nanocomposite films with 5 nm particle size, as observed in Figure 5.8.

The effect of particle size on the state of dispersion for particles having identical functionality can be explained in terms of entropic interactions (i.e. nanoparticle size relative to the radius of gyration). In particle−polymer composites, the polymer chains undergo stretching around the solid nanoparticles, causing a loss in the conformational entropy, which further depends on the particle radius. For large particles, which are entropically disfavored, in the absence of specific interactions, particles are expelled from the bulk of the polymer [49]. This characteristic significantly affects the global distribution of nanoparticles in the polymer matrix.

## 5.2 Electrical Characterization

### 5.2.1 Dielectric Properties of Gold Nanoparticle/PVDF Nanocomposite

To systematically investigate the dielectric properties of the composite films, impedance measurements were made using the semiconductor parameter analyzer on nanocomposite capacitors. Dielectric permittivity values were estimated from the measured capacitance values using the electrode area and film thickness.

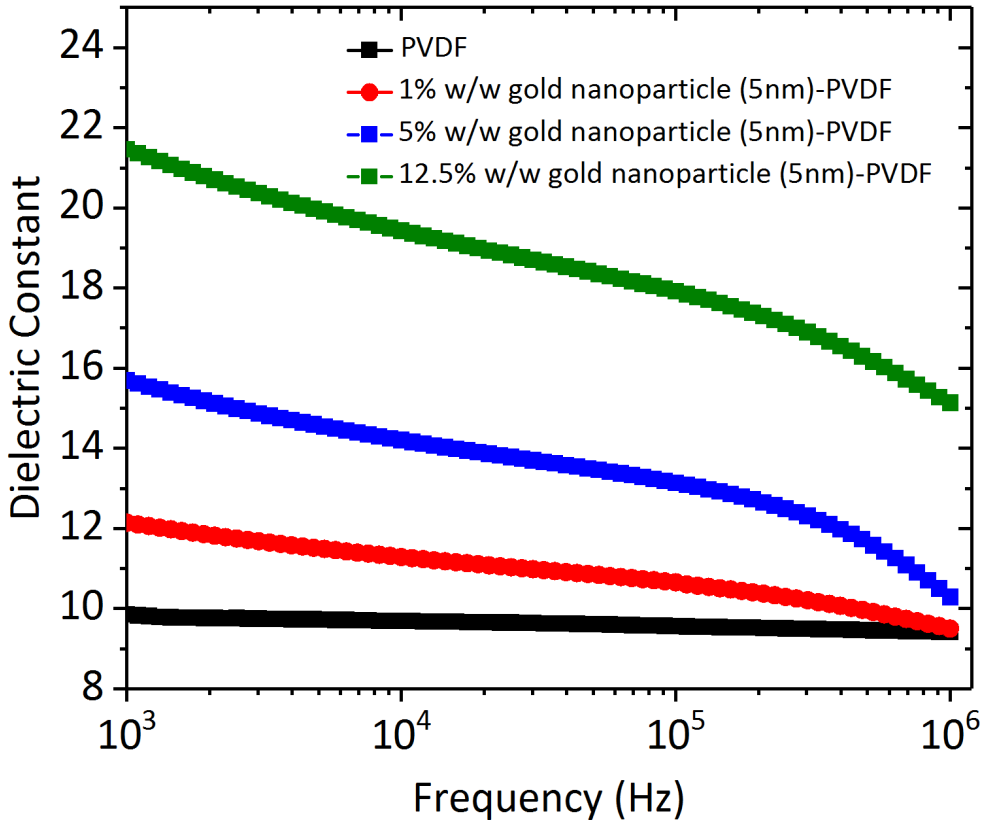


Figure 5.12: Frequency dependent dielectric permittivity for the nanocomposite capacitors with varied gold nanoparticle concentration.

Figure 5.12 shows the variation of the dielectric properties with frequency over the range of 1 kHz to 1 MHz, for nanocomposite films with gold nanoparticle (5 nm) content upto 12.5% w/w. In general, the dielectric permittivity was observed to decrease with the increase in frequency. However, the frequency dependence was weak for nanocomposite films with particle concentration upto 1% w/w. For 5% w/w and 12.5% w/w nanocomposites, the effect of frequency on dielectric permittivity was significant, exhibiting a substantial decrease in dielectric permittivity with the increase in frequency. This is attributed to the space charge polarization between the gold nanoparticles and the PVDF polymer matrix [4]. The dielectric loss can be analyzed in terms of the loss tangent $\tan(\delta)$, also known as the dissipation factor. Loss tangent includes the dissipation due to the resistance in the leads and plates, dielectric damping loss, and conductivity loss of a conductive material. For loss-less material, $\tan(\delta) = 0$. The frequency-dependent response of the loss tangent is shown in Figure 5.13.

For pure PVDF film capacitors, the loss tangent shows frequency-independent characteristics. In case of nanocomposite films, the loss tangent was observed to have weak frequency dependence at low frequency values, but an increase in the loss tangent was observed at higher frequencies ($10^5 - 10^6$ Hz), which might be attributed to the resonance/relaxation

of the host polymer [14, 15, 20, 111, 112] or lead resistance (resistance of the connecting leads). The dissipation due to lead resistance can be expressed as $\omega R_s C$, where $\omega$ is the measurement frequency, $R_s$ is the series resistance due to leads, and C is the capacitance. At high frequencies, when $\omega C$ is large, the dissipation due to lead resistance can dominate the total dissipation, causing an increase in the dissipation factor. This frequency-dependent trend of loss tangent can also be found in previous reports [32–34].

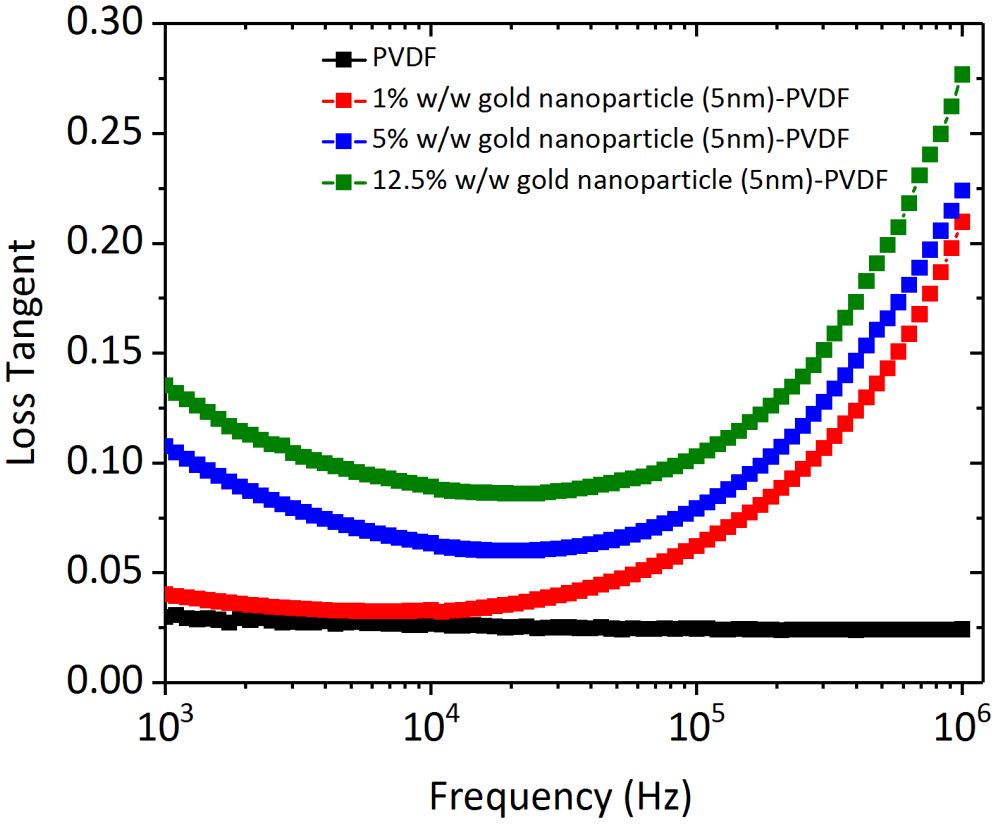


Figure 5.13: Frequency-dependent loss tangent (tan $\delta$) for the nanocomposite capacitors with varied gold nanoparticle concentration.

Figure 5.14 shows the effect of the nanoparticle concentration on the dielectric properties of the nanocomposite materials measured at 1 kHz. The enhancement in the dielectric permittivity increases rapidly when the particle concentration is higher than 1% w/w. A dielectric permittivity of ∼22 was observed at 12.5 % w/w particle content, which is much higher than that of the pure PVDF homopolymer. The effect of the particle concentration on the dielectric loss is illustrated in Figure 5.14. The dielectric loss increased with the increase in the particle concentration in the nanocomposite, probably due to the ohmic current leakage. However, the measured dielectric loss values are quite low, even at high particle concentrations. For example, the loss tangent was measured to be ∼0.14 for 12.5%

w/w nanocomposites. This implies that the gold nanofillers are effectively insulated by the surrounding polymer matrix.

Dielectric measurements were also made for the nanocomposite films embedded with 20 nm gold particles. Figure 5.15 shows the frequency-dependent dielectric permittivity for gold (20 nm)/PVDF nanocomposite films having a nanoparticle concentration of 5% w/w. The dielectric permittivity was observed to decrease with the increase in frequency similar to the case of nanocomposite films containing 5 nm gold nanoparticles as fillers. However, since the nanoparticles were segregated towards the edge of the film rather than being dispersed in the bulk of the polymer matrix (Figure 5.11), the overall enhancement in the dielectric permittivity was not significant. The frequency-dependent loss-tangent for gold (20 nm)/PVDF nanocomposite films having a nanoparticle concentration of 5% w/w is shown in Figure 5.16. Similar to the gold (5 nm)/PVDF nanocomposite case, the loss tangent was observed to have weak frequency dependence at low frequency values, and an increase in the loss tangent was observed at higher frequencies ($10^5 - 10^6$ Hz). The loss-tangent values were relatively higher than the gold (5 nm)/PVDF nanocomposite case. This might be attributed to the agglomeration of gold (20 nm) nanoparticles in the polymer matrix as shown in Figure 5.11.

### 5.2.2 Breakdown Strength of Gold Nanoparticle/PVDF Nanocomposite

The breakdown behavior of the gold nanoparticle/PVDF nanocomposite films was studied by applying a voltage ramp at a rate of 100 V/sec and measuring the resulting current. The current-voltage characteristics of the PVDF film is shown in Figure 5.17. It can be observed that a sharp increase in the current occured at a voltage of 92 V indicating the breakdown of the dielectric film. SEM images of the capacitor devices were obtained after the dielectric breakdown measurements to check the rupture of the film. Figure 5.18 (a) shows the top surface of the dielectric film in lower magnification. The bright circular region in the image corresponds to one of the top electrodes and the surrounding dark area is the polymer film. It can be observed that the dielectric film has ruptured as evident from the several breakdown regions. A high magnification view of one of the breakdown region is shown in Figure 5.18 (b).

For 5% w/w nanocomposite films, a spike in the current was observed at 98 V as shown in Figure 5.19. The breakdown behavior of the 10% w/w nanocomposite film is shown in Figure 5.19. The current rose sharply to 20 milliamperes (mA) at 57 V suggesting the film breakdown. The average breakdown strength for PVDF, 5% and 10% w/w gold nanoparticle/PVDF nanocomposite films is listed in Figure 5.20. The dielectric breakdown strength decreased with the increase in the nanoparticle concentration in the host polymer matrix. However, the decrease in the breakdown strength was not apparent until the particle concentration was increased to 12.5% w/w, where the breakdown strength reduced to 174 MV/m from 269 MV/m (measured for PVDF samples).

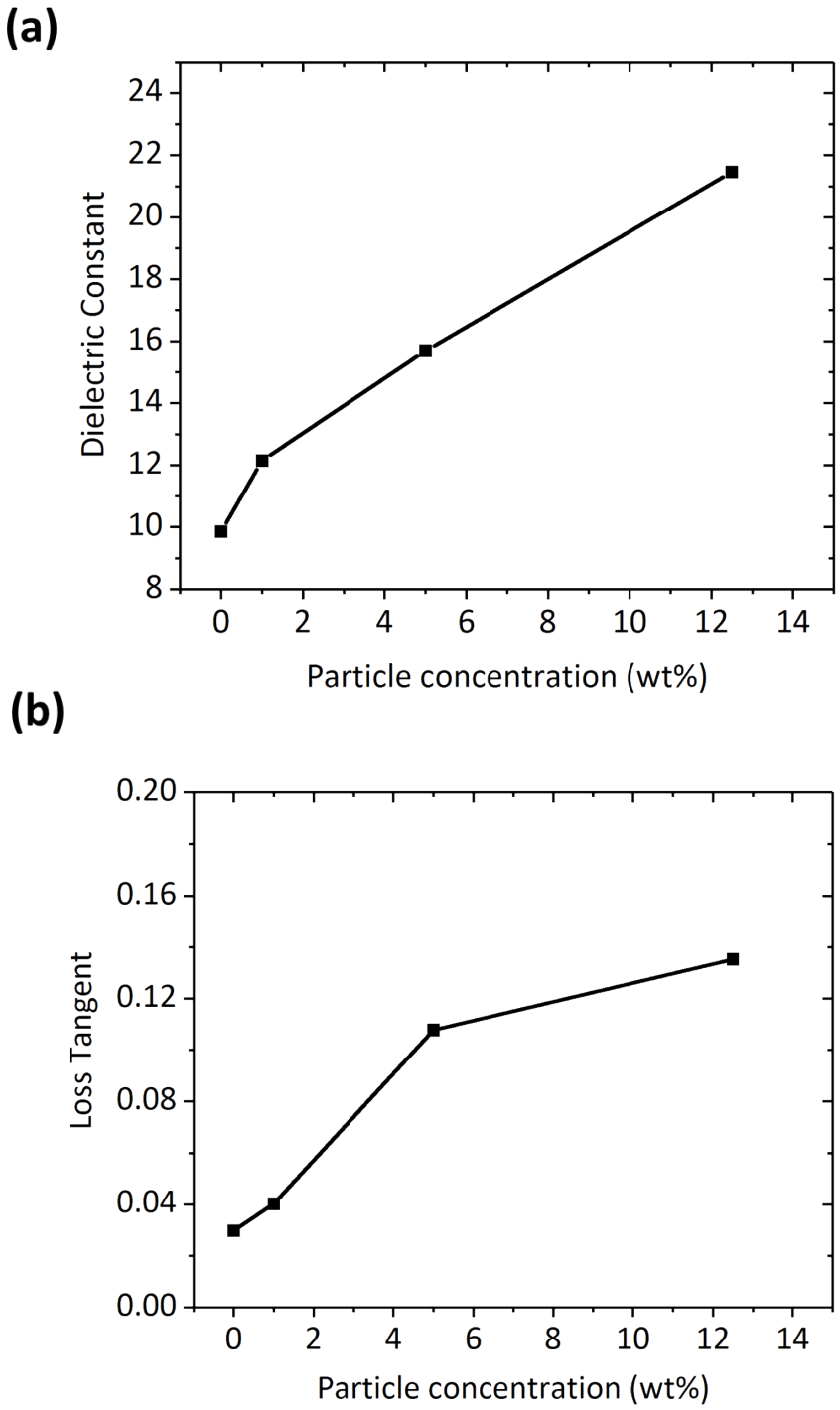


Figure 5.14: Variation of (a) dielectric constant and (b) loss tangent with the filler concentration for gold (5 nm) nanoparticle/PVDF nanocomposite films at 1 kHz.

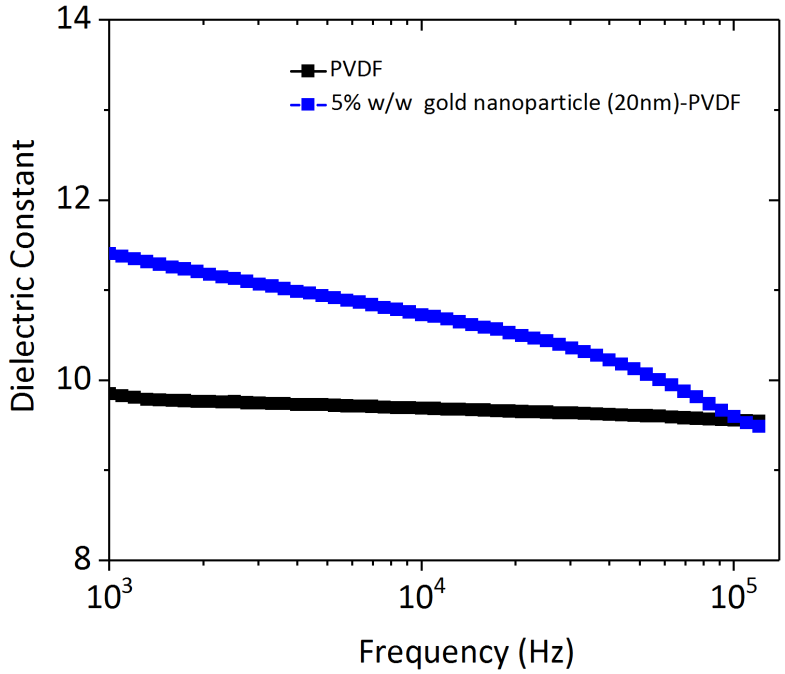


Figure 5.15: Frequency−dependent dielectric permittivity for the gold nanoparticle (20 nm)/PVDF nanocomposite capacitors.

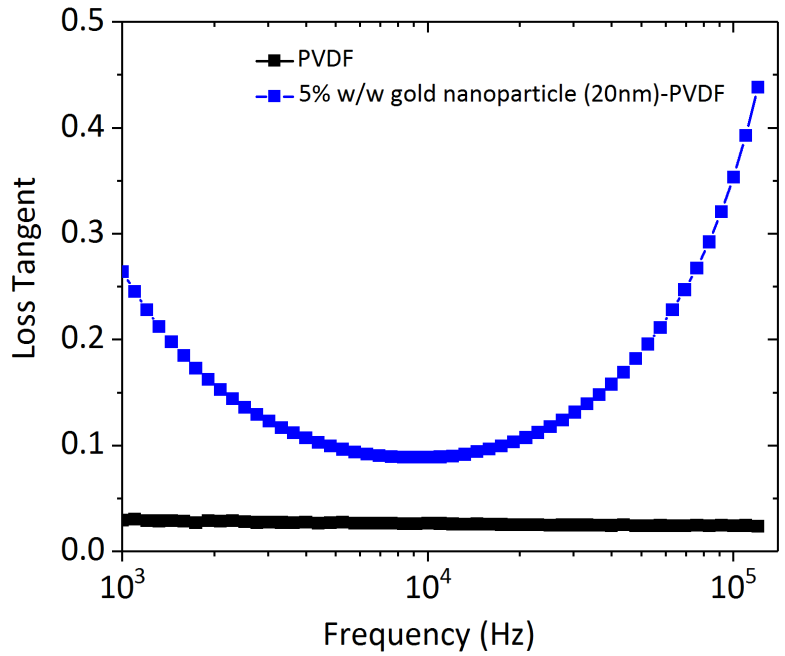


Figure 5.16: Frequency−dependent loss tangent for the gold nanoparticle (20 nm)/PVDF nanocomposite capacitors.

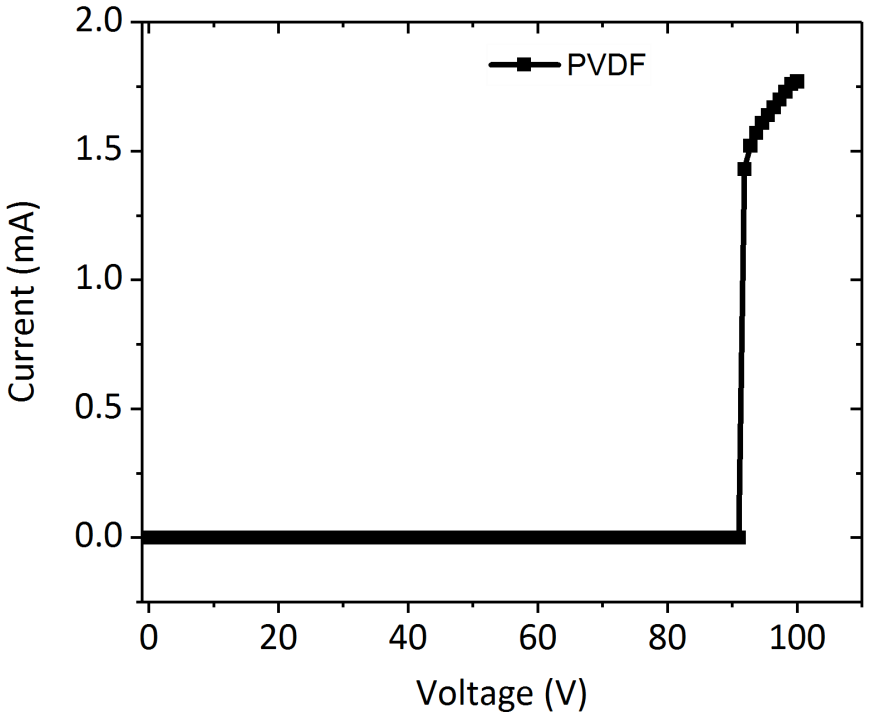


Figure 5.17: Breakdown strength measurement of PVDF films. At $\sim 92$ V the current jumps several orders of magnitude, indicating the breakdown of the PVDF film.

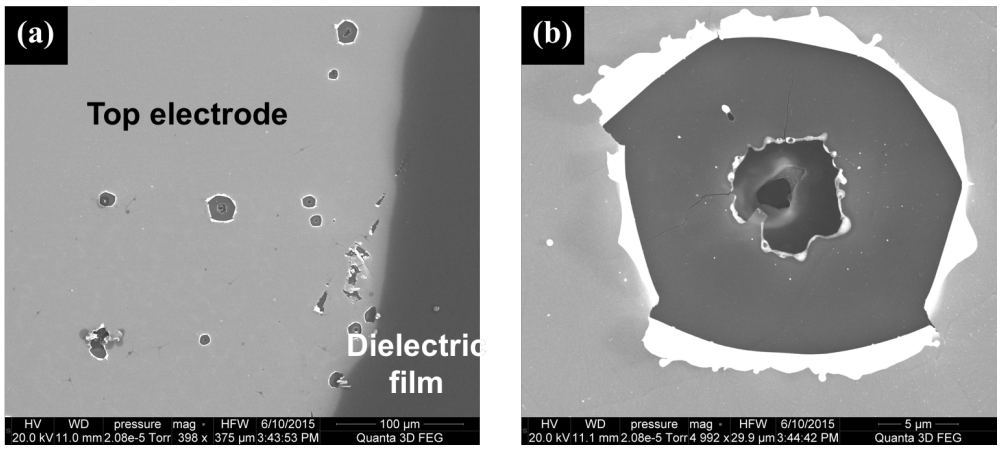


Figure 5.18: SEM images of the capacitor device after the dielectric breakdown strength measurement in (a) low and (b) high magnifications.

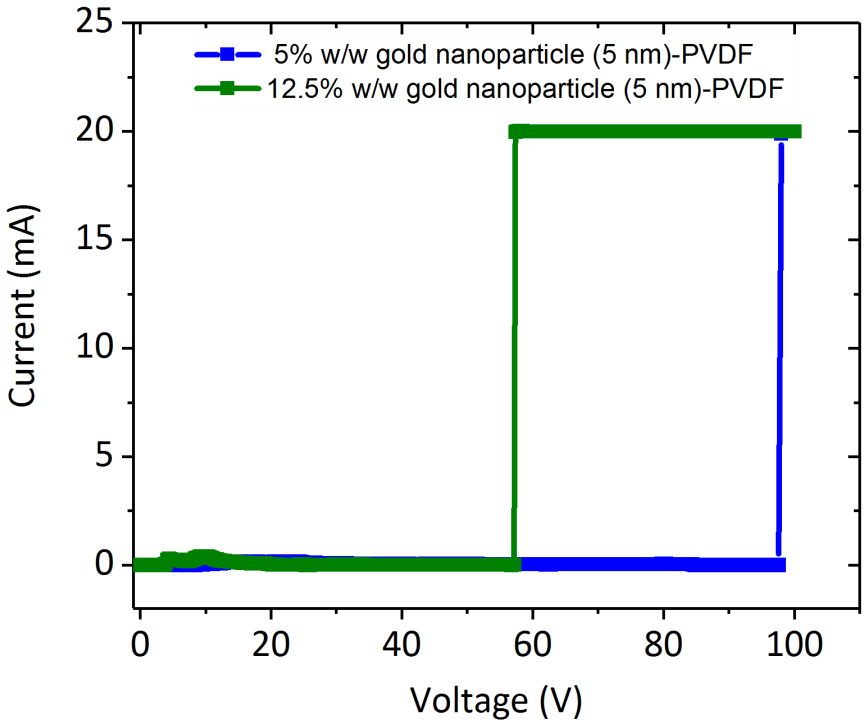


Figure 5.19: Breakdown strength measurement of 5 % and 12.5 % w/w gold nanoparticle (5 nm)/PVDF nanocomposite films. The sharp rise in current at $\sim$ 98 and $\sim$ 57 V indicate the breakdown for 5 wt% and 12.5 wt% nanocomposite films respectively.

| Dielectric Material | Breakdown Strength (MV/m) |
|---|---|
| PVDF | 269 ± 6.4 |
| 5% w/w gold nanoparticle/PVDF | 264 ± 12 |
| 12.5% w/w gold nanoparticle/PVDF | 174 ± 10 |

Figure 5.20: Average breakdown strength values for the gold nanoparticle (5 nm)/PVDF polymer nanocomposite dielectric.

## 5.3 Discussion

In summary, a novel hybrid composite material consisting of PVP-modified gold nanoparticles and PVDF was developed. Nanocomposite films without voids and phase-separation between the particles and polymer phase were successfully synthesized. The electron microscopy images of the gold nanoparticle (5 nm)/PVDF nanocomposite films demonstrated no particle agglomeration up to 12.5% w/w particle concentration. The gold nanoparticle (5 nm)/PVDF nanocomposite films showed high dielectric constant and low dielectric loss, i.e. a dielectric constant value of $\sim 22$ and a loss tangent of $\sim 0.14$ at 1 kHz was measured at a particle concentration of 12.5% w/w. These results provide evidence that enhanced dielectric permittivity can be obtained while low dielectric loss was maintained for polymer composites embedded with ligand-coated metal nanoparticles. In addition, the effect of nanoparticle size on the distribution of gold nanoparticles in the PVDF host polymer and the enhancement of dielectric properties was illustrated.

# Chapter 6

# Conclusions

In this dissertation, solid-state dielectric materials with high dielectric permittivity and low dielectric loss properties were developed to enable high energy density solid-state energy storage mechanisms. Current energy storage systems such as batteries, and supercapacitors offer high energy density in comparison to the conventional solid-state capacitors. However, these systems are liquid/gel based that can explode in extreme thermal conditions, or at higher voltages. Furthermore, their power density is much lower than the conventional-solid state capacitors.

To obtain high dielectric permittivity and low dielectric loss solid-state dielectrics, we proposed the development of novel polymer nanocomposite materials with two key innovations. One involved the 5 nm diameter metal nanoparticle fillers for enhancing the dielectric permittivity of the host polymer matrix and the other pertaining to the selection of the appropriate nanoparticle surface functionalization for controlling particle agglomeration and reducing dielectric loss.

Metal nanoparticles enhance the dielectric permittivity due to the interfacial polarization (also known as Maxwell-Wagner-Sillars polarization) caused by the different relaxation times in particle and polymer phases (i.e., different phases). In particular, 5 nm size particles are chosen to assist in the attainment of homogeneous particle dispersion in the host polymer matrix. In nanoparticle/polymer composite systems, although enthalpic interactions (related to the nanoparticle ligands) are usually dominant, entropic interactions (i.e. nanoparticle size relative to the radius of gyration of polymer) can also play a critical role in controlling particle dispersion. In particle-polymer composites, the polymer chains undergo stretching around the solid nanoparticles, causing a loss in the conformational entropy which further depends on the particle radius. For large particles which are entropically disfavored, in the absence of specific interactions, particles are expelled from the bulk of the polymer. This characteristic significantly affects the global distribution of nanoparticles in the polymer matrix.

This thesis reports the development of two novel polymer nanocomposite dielectric materials one involving PVDF as the host polymer for potential applications in energy storage and the other with SU-8 as the polymer host for microelectronic applications. For each

polymer nanocomposite, the nanoparticle surface functionalization is carefully tailored so as to aid in the dispersion of gold nanoparticles while providing local electrical resistance to allow increased volume fractions of particles in the polymer scaffold.

For the gold nanoparticle/PVDF nanocomposite, PVP-coated gold nanoparticles were embedded in the PVDF polymer matrix. Since PVP is miscible with PVDF, the particle dispersion is enthalpically favored. PVDF has high breakdown strength (>700 MV/m) and the overall dielectric permittivity of nanocomposites was increased owing to nanoscale conductive fillers, thus serving as a high energy density dielectric material. To study the effect of entropic interactions on particle dispersion, nanocomposites with two different particle sizes (5 nm and 20 nm in diameter) were synthesized and characterized. Scanning electron microscopy (SEM), transmission electron microscopy (TEM), and ultramicrotoming techniques were used for the material characterization of the nanocomposite material.

A uniform particle distribution was observed for gold nanoparticle/PVDF nanocomposite films consisting of 5 nm gold particles in contrast to the film with 20 nm particles. Further, the electron microscopy images of the 5 nm gold nanoparticle/PVDF nanocomposite films demonstrated no particle agglomeration up to 12.5% w/w particle concentration. Also, no evidence of macro-phase separation of nanoparticles from the polymer phase was observed. This is important because nanoparticle agglomeration and phase separation from the polymer usually results in poor processability of films and a high defect density. Nanocomposite films without voids and phase-separation between the particles and polymer phase were successfully synthesized. The frequency dependent dielectric permittivity and the loss tangent was studied for the nanocomposite films. The nanocomposite films showed high dielectric constant and low dielectric loss, i.e., a dielectric constant value of 22 and loss tangent of 0.14 at 1 kHz was measured at a particle concentration of 12.5 wt%. These results provide evidence that enhanced dielectric permittivity can be obtained while maintaining the low dielectric loss for polymer composites embedded with coated metal nanoparticles. Such solid-state dielectric materials would enable energy storage solutions having both high energy storage capacity and high power transfer rate. Potential application of the improved energy storage technologies will be across the board from hybrid vehicles requiring fast charge times to consumer electronics demanding longer battery life.

For the gold nanoparticle/SU-8 nanocomposite dielectric, dodecanethiol functionalized gold nanoparticles were embedded in the SU-8 host matrix. The nanocomposite films showed relatively low dielectric loss and considerably high dielectric constant. At a particle concentration of 10% w/w, nanocomposite films exhibited an average dielectric constant of 13.6 and loss tangent of 0.09 at 1 kHz. These results support the use of photodefinable organic polymer composites embedded with functional metal nanoparticles for obtaining enhanced dielectric permittivity while maintaining low dielectric loss. SU-8 based high-k nanocomposite would be an excellent candidate for embedded capacitor applications as it can be easily patterned in the desired shapes using photolithography.

# Chapter 7

# Future Work

The overall conclusions of this thesis indicate that the polymer nanocomposite dielectrics with high dielectric permittivity can be obtained while maintaining low dielectric loss by reducing the agglomeration of the conductive fillers in the host polymer matrix. These solid-state dielectric materials would enable the development of energy storage mechanisms with high energy density and high power density.

As a future work, alternative methods for the fabrication of the polymer nanocomposite dielectric films can be explored to potentially enable the high volume production of the solid-state dielectric materials. Currently, the polymer nanocomposite dielectric films are fabricated on a die-by-die basis using the spin-coating method. Spin coating offers the advantage of good film uniformity and control over the film thickness but it cannot be used for large area processing. Thin film deposition techniques such as doctor blading and dip coating can be explored as they offer large area coverage. Dip coating has the advantage that it can be used to obtain very thin layers. These studies would entail investigation of the state of the nanoparticle dispersion in the resulting nanocomposite films and the measurement of the dielectric properties for comparative analysis.

Finally for the photodefinable polymer nanocomposites, to further enhance their dielectric permittivity, the gold nanoparticle dispersion in the SU-8 photopolymer can be further improved. Alternative surface functionalization groups or polymer brushes on the gold nanoparticle surface can be attached to improve the wettabiliity of the nanofillers in the SU-8 polymer matrix. This would allow the addition of the gold nanoparticles in increased volume fractions in the polymer matrix yielding enhanced dielectric performance.

# Bibliography


[1] Mohsen Ahmadipour, Mohd Fadzil Ain, and Zainal Arifin Ahmad. "A short review on copper calcium titanate (CCTO) electroceramic: synthesis, dielectric properties, film deposition, and sensing application". In: *Nano-Micro Letters* 8.4 (2016), pp. 291–311 (cit. on p. 1).

[2] Peter Barber, Shiva Balasubramanian, Yogesh Anguchamy, Shushan Gong, Arief Wibowo, Hongsheng Gao, Harry J Ploehn, and Hans-Conrad Zur Loye. "Polymer composite and nanocomposite dielectric materials for pulse power energy storage". In: *Materials* 2.4 (2009), pp. 1697–1733 (cit. on p. 1).

[3] Carole Jacques. *Energy Storage Market Rises to $50 Billion in 2020, amid Dramatic Changes*. URL: `http://www.luxresearchinc.com/news-and-events/press-releases/read/energy-storage-market-rises-50-billion-2020-amid-dramatic` (cit. on p. 2).

[4] Keun Hyung Lee, Joseph Kao, Saman Salemizadeh Parizi, Gabriel Caruntu, and Ting Xu. "Dielectric properties of barium titanate supramolecular nanocomposites". In: *Nanoscale* 6.7 (2014), pp. 3526–3531 (cit. on pp. 2, 50).

[5] GM Ouyang, KY Wang, and XY Chen. "Enhanced electro-mechanical performance of TiO 2 nano-particle modified polydimethylsiloxane (PDMS) as electroactive polymers". In: *Solid-State Sensors, Actuators and Microsystems Conference (TRANSDUCERS), 2011 16th International*. IEEE. 2011, pp. 614–617 (cit. on p. 2).

[6] Tetsuji Inui, Hirotaka Koga, Masaya Nogi, Natsuki Komoda, and Katsuaki Suganuma. "High-dielectric paper composite consisting of cellulose nanofiber and silver nanowire". In: *Nanotechnology (IEEE-NANO), 2014 IEEE 14th International Conference on*. IEEE. 2014, pp. 470–473 (cit. on p. 2).

[7] Dong Kee Yi, Su Seong Lee, and Jackie Y Ying. "Synthesis and applications of magnetic nanocomposite catalysts". In: *Chemistry of materials* 18.10 (2006), pp. 2459–2461 (cit. on p. 2).

[8] P Markondeya Raj, Parthasarathi Chakraborti, Himani Sharma, KyuHwan Han, Saumya Gandhi, Srikrishna Sitaraman, Madhavan Swaminathan, and Rao Tummala. "Tunable and miniaturized RF components with nanocomposite and nanolayered

dielectrics". In: *Nanotechnology (IEEE-NANO), 2014 IEEE 14th International Conference on*. IEEE. 2014, pp. 27–31 (cit. on p. 2).

[9] Xin Li, Meixiang Wan, Yen Wei, Jiaoyan Shen, and Zhaojia Chen. "Electromagnetic functionalized and core- shell micro/nanostructured polypyrrole composites". In: *The Journal of Physical Chemistry B* 110.30 (2006), pp. 14623–14626 (cit. on p. 2).

[10] Mohammad Rajib, Ricardo Martinez, Mohammad Shuvo, Hasanul Karim, Diego Delfin, Samia Afrin, Gerardo Rodriguez, Ramana Chintalapalle, and Yirong Lin. "Enhanced energy storage of dielectric nanocomposites at elevated temperatures". In: *International Journal of Applied Ceramic Technology* 13.1 (2016), pp. 125–132 (cit. on p. 2).

[11] Liyuan Xie, Xingyi Huang, Yanhui Huang, Ke Yang, and Pingkai Jiang. "Core@ double-shell structured BaTiO3–polymer nanocomposites with high dielectric constant and low dielectric loss for energy storage application". In: *The Journal of Physical Chemistry C* 117.44 (2013), pp. 22525–22537 (cit. on p. 2).

[12] V Tomer, G Polizos, E Manias, and CA Randall. "Epoxy-based nanocomposites for electrical energy storage. I: Effects of montmorillonite and barium titanate nanofillers". In: *Journal of Applied Physics* 108.7 (2010), p. 074116 (cit. on p. 2).

[13] Junjun Li, Jason Claude, Luis Enrique Norena-Franco, Sang Il Seok, and Qing Wang. "Electrical energy storage in ferroelectric polymer nanocomposites containing surface-functionalized BaTiO3 nanoparticles". In: *Chemistry of Materials* 20.20 (2008), pp. 6304–6306 (cit. on p. 3).

[14] Haixiong Tang, Yirong Lin, Clark Andrews, and Henry A Sodano. "Nanocomposites with increased energy density through high aspect ratio PZT nanowires". In: *Nanotechnology* 22.1 (2010), p. 015702 (cit. on pp. 3, 51).

[15] Philseok Kim, Natalie M Doss, John P Tillotson, Peter J Hotchkiss, Ming-Jen Pan, Seth R Marder, Jiangyu Li, Jeffery P Calame, and Joseph W Perry. "High energy density nanocomposites based on surface-modified BaTiO3 and a ferroelectric polymer". In: *ACS nano* 3.9 (2009), pp. 2581–2592 (cit. on pp. 3, 29, 51).

[16] Haixiong Tang and Henry A Sodano. "Ultra high energy density nanocomposite capacitors with fast discharge using Ba0. 2Sr0. 8TiO3 nanowires". In: *Nano letters* 13.4 (2013), pp. 1373–1379 (cit. on p. 3).

[17] Haixiong Tang, Yirong Lin, and Henry A Sodano. "Synthesis of high aspect ratio batio3 nanowires for high energy density nanocomposite capacitors". In: *Advanced Energy Materials* 3.4 (2013), pp. 451–456 (cit. on p. 3).

[18] Yang Shen, Yuanhua Lin, Ming Li, and C-W Nan. "High dielectric performance of polymer composite films induced by a percolating interparticle barrier layer". In: *Advanced Materials* 19.10 (2007), pp. 1418–1422 (cit. on p. 3).

[19] C-W Nan, Y Shen, and Jing Ma. "Physical properties of composites near percolation". In: *Annual Review of Materials Research* 40 (2010), pp. 131–151 (cit. on pp. 3, 39).

[20] Jiaming Zhu, Jiabin Shen, Shaoyun Guo, and Hung-Jue Sue. "Confined distribution of conductive particles in polyvinylidene fluoride-based multilayered dielectrics: Toward high permittivity and breakdown strength". In: *Carbon* 84 (2015), pp. 355–364 (cit. on pp. 3, 39, 51).

[21] Ana Cazacu, Lavinia Curecheriu, Alexandra Neagu, Leontin Padurariu, Adrian Cernescu, Isabelle Lisiecki, and Liliana Mitoseriu. "Tunable gold-chitosan nanocomposites by local field engineering". In: *Applied Physics Letters* 102.22 (2013), p. 222903 (cit. on p. 3).

[22] IA Tchmutin, AT Ponomarenko, EP Krinichnaya, GI Kozub, and ON Efimov. "Electrical properties of composites based on conjugated polymers and conductive fillers". In: *Carbon* 41.7 (2003), pp. 1391–1395 (cit. on p. 3).

[23] Hristiyan Stoyanov, Denis Mc Carthy, Matthias Kollosche, and Guggi Kofod. "Dielectric properties and electric breakdown strength of a subpercolative composite of carbon black in thermoplastic copolymer". In: *Applied physics letters* 94.23 (2009), p. 232905 (cit. on p. 3).

[24] Koichi Suematsu, Masashi Arimura, Naoyuki Uchiyama, Shingo Saita, and Teruhisa Makino. "High-performance dielectric thin film nanocomposites of barium titanate and cyanoethyl pullulan: controlling the barium titanate nanoparticle size using a sol–gel method". In: *RSC Advances* 6.25 (2016), pp. 20807–20813 (cit. on p. 3).

[25] Nao Kamezawa, Daisuke Nagao, Haruyuki Ishii, and Mikio Konno. "Transparent, highly dielectric poly (vinylidene fluoride) nanocomposite film homogeneously incorporating BaTiO 3 nanoparticles with fluoroalkylsilane surface modifier". In: *European Polymer Journal* 66 (2015), pp. 528–532 (cit. on p. 3).

[26] Yifei Wang, Jin Cui, Qibin Yuan, Yujuan Niu, Yuanyuan Bai, and Hong Wang. "Significantly Enhanced Breakdown Strength and Energy Density in Sandwich-Structured Barium Titanate/Poly (vinylidene fluoride) Nanocomposites". In: *Advanced Materials* 27.42 (2015), pp. 6658–6663 (cit. on p. 3).

[27] Xiang Lin, Penghao Hu, Zhuye Jia, and Shengmin Gao. "Enhanced electric displacement induces large energy density in polymer nanocomposites containing core–shell structured BaTiO 3@ TiO 2 nanofibers". In: *Journal of Materials Chemistry A* 4.6 (2016), pp. 2314–2320 (cit. on p. 3).

[28] Glyn J Reynolds, Martin Kratzer, Martin Dubs, Heinz Felzer, and Robert Mamazza. "Electrical properties of thin-film capacitors fabricated using high temperature sputtered modified barium titanate". In: *Materials* 5.4 (2012), pp. 644–660 (cit. on p. 3).

[29] Fajun Wang, Dongxiang Zhou, and Shuping Gong. "Dielectric behavior of TIC–PVDF nanocomposites". In: *physica status solidi (RRL)-Rapid Research Letters* 3.1 (2009), pp. 22–24 (cit. on p. 3).

[30] Jianjun Liu, Robert W Smith, and Wai-Ning Mei. "Synthesis of the giant dielectric constant material CaCu3Ti4O12 by wet-chemistry methods". In: *Chemistry of Materials* 19.24 (2007), pp. 6020–6024 (cit. on p. 3).

[31] Jin-Kai Yuan, Zhi-Min Dang, Sheng-Hong Yao, Jun-Wei Zha, Tao Zhou, Sheng-Tao Li, and Jinbo Bai. "Fabrication and dielectric properties of advanced high permittivity polyaniline/poly (vinylidene fluoride) nanohybrid films with high energy storage density". In: *Journal of Materials Chemistry* 20.12 (2010), pp. 2441–2447 (cit. on p. 3).

[32] Cheng Yang, Hong-song Song, and Da-bo Liu. "Effect of coupling agents on the dielectric properties of CaCu 3 Ti 4 O 12/PVDF composites". In: *Composites Part B: Engineering* 50 (2013), pp. 180–186 (cit. on pp. 4, 51).

[33] Khurram Shehzad, Asad Ul-Haq, Shahabaz Ahmad, Muhamamd Mumtaz, Tajamal Hussain, Adnan Mujahid, Asma Tufail Shah, Muhammad Yasir Choudhry, Irshad Khokhar, Sadaf Ul-Hassan, et al. "All-organic PANI–DBSA/PVDF dielectric composites with unique electrical properties". In: *Journal of Materials Science* 48.10 (2013), pp. 3737–3744 (cit. on pp. 4, 51).

[34] Claudia Ehrhardt, Christian Fettkenhauer, Jens Glenneberg, Wolfram Münchgesang, Hartmut S Leipner, Martin Diestelhorst, Sebastian Lemm, Horst Beige, and Stefan G Ebbinghaus. "A solution-based approach to composite dielectric films of surface functionalized CaCu 3 Ti 4 O 12 and P (VDF-HFP)". In: *Journal of Materials Chemistry A* 2.7 (2014), pp. 2266–2274 (cit. on pp. 4, 51).

[35] TJ Lewis. "Interfaces: nanometric dielectrics". In: *Journal of Physics D: Applied Physics* 38.2 (2005), p. 202 (cit. on pp. 4, 5).

[36] TJ Lewis. "Interfaces are the dominant feature of dielectrics at the nanometric level". In: *IEEE Transactions on Dielectrics and Electrical Insulation* 11.5 (2004), pp. 739–753 (cit. on pp. 4, 5).

[37] RC Smith, C Liang, M Landry, JK Nelson, and LS Schadler. "The mechanisms leading to the useful electrical properties of polymer nanodielectrics". In: *IEEE Transactions on Dielectrics and Electrical Insulation* 15.1 (2008) (cit. on p. 5).

[38] M Roy, JK Nelson, RK MacCrone, Linda S Schadler, CW Reed, and Richard Keefe. "Polymer nanocomposite dielectrics-the role of the interface". In: *IEEE Transactions on Dielectrics and Electrical Insulation* 12.4 (2005), pp. 629–643 (cit. on p. 5).

[39] Sasidhar Siddabattuni, Thomas P Schuman, and Fatih Dogan. "Dielectric properties of polymer–particle nanocomposites influenced by electronic nature of filler surfaces". In: *ACS applied materials & interfaces* 5.6 (2013), pp. 1917–1927 (cit. on p. 5).

[40] Chatchai Putson, Laurent Lebrun, Daniel Guyomar, Nantakan Muensit, P-J Cottinet, Laurence Seveyrat, and Benoit Guiffard. "Effects of copper filler sizes on the dielectric properties and the energy harvesting capability of nonpercolated polyurethane composites". In: *Journal of Applied Physics* 109.2 (2011), p. 024104 (cit. on p. 5).

[41] Michael E Mackay, Anish Tuteja, Phillip M Duxbury, Craig J Hawker, Brooke Van Horn, Zhibin Guan, Guanghui Chen, and RS Krishnan. "General strategies for nanoparticle dispersion". In: *Science* 311.5768 (2006), pp. 1740–1743 (cit. on pp. 5, 9, 10).

[42] Kyle C Bryson. "Controlling the Assembly of Nanoparticles in Polymer Blends". In: (2016) (cit. on p. 5).

[43] S Diaham, S Zelmat, M-L Locatelli, S Dinculescu, M Decup, and T Lebey. "Dielectric breakdown of polyimide films: Area, thickness and temperature dependence". In: *IEEE Transactions on Dielectrics and Electrical Insulation* 17.1 (2010) (cit. on p. 6).

[44] J Artbauer. "Electric strength of polymers". In: *Journal of Physics D: Applied Physics* 29.2 (1996), p. 446 (cit. on p. 6).

[45] Masayuki Ieda. "Dielectric breakdown process of polymers". In: *IEEE Transactions on Electrical Insulation* 3 (1980), pp. 206–224 (cit. on p. 6).

[46] Saumil P Samant, Christopher A Grabowski, Kim Kisslinger, Kevin G Yager, Guangcui Yuan, Sushil K Satija, Michael F Durstock, Dharmaraj Raghavan, and Alamgir Karim. "Directed self-assembly of block copolymers for high breakdown strength polymer film capacitors". In: *ACS applied materials & interfaces* 8.12 (2016), pp. 7966–7976 (cit. on p. 6).

[47] Justin B Hooper and Kenneth S Schweizer. "Theory of phase separation in polymer nanocomposites". In: *Macromolecules* 39.15 (2006), pp. 5133–5142 (cit. on p. 9).

[48] Bo Gao, Matthew J Rozin, and Andrea R Tao. "Plasmonic nanocomposites: polymer-guided strategies for assembling metal nanoparticles". In: *Nanoscale* 5.13 (2013), pp. 5677–5691 (cit. on p. 9).

[49] Russell B Thompson, Valeriy V Ginzburg, Mark W Matsen, and Anna C Balazs. "Predicting the mesophases of copolymer-nanoparticle composites". In: *Science* 292.5526 (2001), pp. 2469–2472 (cit. on pp. 10, 49).

[50] Daniel Sunday, Jan Ilavsky, and David L Green. "A phase diagram for polymer-grafted nanoparticles in homopolymer matrices". In: *Macromolecules* 45.9 (2012), pp. 4007–4011 (cit. on p. 10).

[51] Amalie L Frischknecht, Michael JA Hore, Jamie Ford, and Russell J Composto. "Dispersion of polymer-grafted nanorods in homopolymer films: theory and experiment". In: *Macromolecules* 46.7 (2013), pp. 2856–2869 (cit. on p. 10).

[52] Suresh Gupta, Qingling Zhang, Todd Emrick, Anna C Balazs, and Thomas P Russell. "Entropy-driven segregation of nanoparticles to cracks in multilayered composite polymer structures". In: *Nature Materials* 5.3 (2006), pp. 229–233 (cit. on p. 10).

[53] Pinar Akcora, Hongjun Liu, Sanat K Kumar, Joseph Moll, Yu Li, Brian C Benicewicz, Linda S Schadler, Devrim Acehan, Athanassios Z Panagiotopoulos, Victor Pryamitsyn, et al. "Anisotropic self-assembly of spherical polymer-grafted nanoparticles". In: *Nature materials* 8.4 (2009), pp. 354–359 (cit. on p. 10).

[54] Lejun Qi, Linnea Petersson, and Tieliang Liu. "Review of recent activities on dielectric films for capacitor applications". In: *Journal of International Council on Electrical Engineering* 4.1 (2014), pp. 1–6 (cit. on p. 11).

[55] Jiongxin Lu and CP Wong. "Recent advances in high-k nanocomposite materials for embedded capacitor applications". In: *IEEE Transactions on Dielectrics and Electrical Insulation* 15.5 (2008) (cit. on p. 11).

[56] Joost Melai, Cora Salm, Sander Smits, Jan Visschers, and Jurriaan Schmitz. "The electrical conduction and dielectric strength of SU-8". In: *Journal of Micromechanics and Microengineering* 19.6 (2009), p. 065012 (cit. on p. 11).

[57] I Roch, Ph Bidaud, D Collard, and L Buchaillot. "Fabrication and characterization of an SU-8 gripper actuated by a shape memory alloy thin film". In: *Journal of Micromechanics and Microengineering* 13.2 (2003), p. 330 (cit. on p. 12).

[58] R Feng and RJ Farris. "The characterization of thermal and elastic constants for an epoxy photoresist SU8 coating". In: *Journal of materials science* 37.22 (2002), pp. 4793–4799 (cit. on p. 12).

[59] Hexion. *EPON Resin SU-8, Technical Data Sheet* (cit. on p. 12).

[60] LJ Guerin, M Bossel, Michel Demierre, S Calmes, and Philippe Renaud. "Simple and low cost fabrication of embedded microchannels by using a new thick-film photoplastic". In: *Transducers*. Vol. 97. 1997, pp. 1419–1422 (cit. on p. 12).

[61] KY Lee, N LaBianca, SA Rishton, S Zolgharnain, JD Gelorme, J Shaw, and TH-P Chang. "Micromachining applications of a high resolution ultrathick photoresist". In: *Journal of Vacuum Science & Technology B* 13.6 (1995), pp. 3012–3016 (cit. on p. 12).

[62] Microchem. *SU-8 table of properties*. URL: `http://www.microchem.com/pdf/SU-8-table-of-properties.pdf` (cit. on p. 12).

[63] JR Thorpe, DP Steenson, and RE Miles. "High frequency transmission line using micromachined polymer dielectric". In: *Electronics Letters* 34.12 (1998), pp. 1237–1238 (cit. on p. 12).

[64] S Arscott, F Garet, P Mounaix, L Duvillaret, J-L Coutaz, and D Lippens. "Terahertz time-domain spectroscopy of films fabricated from SU-8". In: *Electronics Letters* 35.3 (1999), pp. 243–244 (cit. on p. 12).

[65] Mi-Zi Li, Jian-Hua Li, Xi-Sheng Shao, Jing Miao, Jia-Bin Wang, Qi-Qing Zhang, and Xiao-Ping Xu. "Grafting zwitterionic brush on the surface of PVDF membrane using physisorbed free radical grafting technique". In: *Journal of membrane science* 405 (2012), pp. 141–148 (cit. on p. 13).

[66] Kai Yu Wang, Tai-Shung Chung, and Marek Gryta. "Hydrophobic PVDF hollow fiber membranes with narrow pore size distribution and ultra-thin skin for the fresh water production through membrane distillation". In: *Chemical Engineering Science* 63.9 (2008), pp. 2587–2594 (cit. on p. 13).

[67] May May Teoh, Tai-Shung Chung, and Yan Shan Yeo. "Dual-layer PVDF/PTFE composite hollow fibers with a thin macrovoid-free selective layer for water production via membrane distillation". In: *Chemical engineering journal* 171.2 (2011), pp. 684–691 (cit. on p. 13).

[68] Supakorn Atchariyawut, Chunsheng Feng, Rong Wang, Ratana Jiraratananon, and DT Liang. "Effect of membrane structure on mass-transfer in the membrane gas–liquid contacting process using microporous PVDF hollow fibers". In: *Journal of Membrane Science* 285.1 (2006), pp. 272–281 (cit. on p. 13).

[69] Deyin Hou, Jun Wang, Xiangcheng Sun, Zhongguang Ji, and Zhaokun Luan. "Preparation and properties of PVDF composite hollow fiber membranes for desalination through direct contact membrane distillation". In: *Journal of membrane science* 405 (2012), pp. 185–200 (cit. on p. 13).

[70] Baojin Chu, Xin Zhou, Kailiang Ren, Bret Neese, Minren Lin, Qing Wang, F Bauer, and QM Zhang. "A dielectric polymer with high electric energy density and fast discharge speed". In: *Science* 313.5785 (2006), pp. 334–336 (cit. on p. 13).

[71] Marcel Benz and William B Euler. "Determination of the crystalline phases of poly (vinylidene fluoride) under different preparation conditions using differential scanning calorimetry and infrared spectroscopy". In: *Journal of applied polymer science* 89.4 (2003), pp. 1093–1100 (cit. on p. 13).

[72] Rinaldo Gregorio. "Determination of the $\alpha$, $\beta$, and $\gamma$ crystalline phases of poly (vinylidene fluoride) films prepared at different conditions". In: *Journal of Applied Polymer Science* 100.4 (2006), pp. 3272–3279 (cit. on p. 13).

[73] Sigma-Aldrich. *PVDF product specification*. URL: `http://www.sigmaaldrich.com/Graphics/COfAInfo/SigmaSAPQM/SPEC/42/427152/427152-BULK_____ALDRICH__.pdf` (cit. on p. 14).

[74] E Fontananova, MA Bahattab, SA Aljlil, M Alowairdy, G Rinaldi, D Vuono, JB Nagy, E Drioli, and G Di Profio. "From hydrophobic to hydrophilic polyvinylidene-fluoride (PVDF) membranes by gaining new insight into material's properties". In: *RSC Advances* 5.69 (2015), pp. 56219–56231 (cit. on p. 14).

[75] EJA Pope, M Asami, and JD Mackenzie. "Transparent silica gel–PMMA composites". In: *Journal of Materials Research* 4.04 (1989), pp. 1018–1026 (cit. on p. 17).

[76] Ou Yuchun, Yang Feng, and Chen Jin. "Interfacial interaction and mechanical properties of nylon 6-potassium titanate composites prepared by in-situ polymerization". In: *Journal of applied polymer science* 64.12 (1997), pp. 2317–2322 (cit. on p. 17).

[77] Feng Yang, Yuchun Ou, and Zhongzhen Yu. "Polyamide 6/silica nanocomposites prepared by in situ polymerization". In: *Journal of Applied Polymer Science* 69.2 (1998), pp. 355–361 (cit. on p. 17).

[78] Katrin Scharlach and Walter Kaminsky. "New Polyolefin-Nanocomposites by In Situ Polymerization with Metallocene Catalysts". In: *Macromolecular symposia*. Vol. 261. 1. Wiley Online Library. 2008, pp. 10–17 (cit. on p. 17).

[79] Yoshiki Chujo and Takeo Saegusa. "Organic polymer hybrids with silica gel formed by means of the sol-gel method". In: *Macromolecules: Synthesis, Order and Advanced Properties* (1992), pp. 11–29 (cit. on p. 18).

[80] Bruce M Novak. "Hybrid nanocomposite materialsbetween inorganic glasses and organic polymers". In: *Advanced Materials* 5.6 (1993), pp. 422–433 (cit. on p. 18).

[81] K Haraguchi, Y Usami, K Yamamura, and S Matsumoto. "Morphological investigation of hybrid materials composed of phenolic resin and silica prepared by in situ polymerization". In: *Polymer* 39.25 (1998), pp. 6243–6250 (cit. on p. 18).

[82] Yoshiki Chujo and Ryo Tamaki. "New preparation methods for organic–inorganic polymer hybrids". In: *MRS Bulletin* 26.05 (2001), pp. 389–392 (cit. on p. 18).

[83] Hideki Goda and Curtis W Frank. "Fluorescence studies of the hybrid composite of segmented-polyurethane and silica". In: *Chemistry of materials* 13.9 (2001), pp. 2783–2787 (cit. on p. 18).

[84] Ryo Tamaki, Yoshiki Chujo, Koji Kuraoka, and Tetsuo Yazawa. "Application of organic-inorganic polymer hybrids as selective gas permeation membranes". In: *Journal of Materials Chemistry* 9.8 (1999), pp. 1741–1746 (cit. on p. 18).

[85] Barry Luther-Davies, Marek Samoc, and Maneerat Woodruff. "Comparison of the Linear and Nonlinear Optical Properties of Poly (p-phenylenevinylene)/Sol- Gel Composites Derived from Tetramethoxysilane and Methyltrimethoxysilane". In: *Chemistry of materials* 8.11 (1996), pp. 2586–2594 (cit. on p. 18).

[86] Jens Christoph Natterodt, Janak Sapkota, E Johan Foster, and Christoph Weder. "Polymer Nanocomposites with Cellulose Nanocrystals Featuring Adaptive Surface Groups". In: *Biomacromolecules* (2017) (cit. on p. 18).

[87] Kyriaki Kalaitzidou, Hiroyuki Fukushima, and Lawrence T Drzal. "A new compounding method for exfoliated graphite–polypropylene nanocomposites with enhanced flexural properties and lower percolation threshold". In: *Composites Science and Technology* 67.10 (2007), pp. 2045–2051 (cit. on p. 18).

[88] Feng Yang and Gordon L Nelson. "Polymer/silica nanocomposites prepared via extrusion". In: *Polymers for advanced technologies* 17.4 (2006), pp. 320–326 (cit. on p. 18).

[89] JW Ess and PR Hornsby. "Twin-screw extrusion compounding of mineral filled thermoplastics: Dispersive mixing effects". In: *Plastics and rubber processing and applications* 8.3 (1987), pp. 147–156 (cit. on p. 18).

[90] Stan Jakopin. "Compounding of additives". In: *Proceedings of 37th Annual SPE Technical Conference (ANTEC 1979 Conference)*. 1979, pp. 987–991 (cit. on p. 18).

[91] Rodney Andrews, David Jacques, Dali Qian, and Terry Rantell. "Multiwall carbon nanotubes: synthesis and application". In: *Accounts of Chemical Research* 35.12 (2002), pp. 1008–1017 (cit. on p. 18).

[92] US Agarwal, Anuya Nisal, Rani Joseph, et al. "PET-SWNT nanocomposites through ultrasound assisted dissolution-evaporation". In: *European Polymer Journal* 43.6 (2007), pp. 2279–2285 (cit. on p. 18).

[93] Dong Wook Chae and Byoung Chul Kim. "Characterization on polystyrene/zinc oxide nanocomposites prepared from solution mixing". In: *Polymers for advanced technologies* 16.11-12 (2005), pp. 846–850 (cit. on p. 18).

[94] Wei Pan and Hantao Zou. "Characterization of PAN/ATO nanocomposites prepared by solution blending". In: *Bulletin of Materials Science* 31.5 (2008), pp. 807–811 (cit. on p. 18).

[95] Michele Preghenella, Alessandro Pegoretti, and Claudio Migliaresi. "Thermo-mechanical characterization of fumed silica-epoxy nanocomposites". In: *Polymer* 46.26 (2005), pp. 12065–12072 (cit. on p. 18).

[96] Mitsuru Tanahashi. "Development of fabrication methods of filler/polymer nanocomposites: With focus on simple melt-compounding-based approach without surface modification of nanofillers". In: *Materials* 3.3 (2010), pp. 1593–1619 (cit. on p. 19).

[97] Maria M Pérez-Madrigal, Elaine Armelin, Jordi Puiggalí, and Carlos Alemán. "Insulating and semiconducting polymeric free-standing nanomembranes with biomedical applications". In: *Journal of Materials Chemistry B* 3.29 (2015), pp. 5904–5932 (cit. on p. 20).

[98] Hemant Kumar Raut, V Anand Ganesh, A Sreekumaran Nair, and Seeram Ramakrishna. "Anti-reflective coatings: A critical, in-depth review". In: *Energy & Environmental Science* 4.10 (2011), pp. 3779–3804 (cit. on p. 21).

[99] Hongta Yang and Peng Jiang. "Large-scale colloidal self-assembly by doctor blade coating". In: *Langmuir* 26.16 (2010), pp. 13173–13182 (cit. on p. 22).

[100] Irshad Hussain, Susan Graham, Zhenxin Wang, Bien Tan, David C Sherrington, Steven P Rannard, Andrew I Cooper, and Mathias Brust. "Size-controlled synthesis of near-monodisperse gold nanoparticles in the 1- 4 nm range using polymeric stabilizers". In: *Journal of the American Chemical Society* 127.47 (2005), pp. 16398–16399 (cit. on p. 26).

[101] Anju Toor, Hongyun So, and Albert P Pisano. "Dielectric properties of ligand-modified gold nanoparticles/SU-8 photopolymer based nanocomposites". In: *Applied Surface Science* (2017) (cit. on p. 27).

[102] Anju Toor, Jim C Cheng, and Albert P Pisano. "Synthesis and characterization of gold nanoparticle/SU-8 polymer based nanocomposite". In: *Nano/Micro Engineered and Molecular Systems (NEMS), 2014 9th IEEE International Conference on*. IEEE. 2014, pp. 664–668 (cit. on pp. 27, 29).

[103] Alexia Gobrecht, Ryad Bendoula, Jean-Michel Roger, and Véronique Bellon-Maurel. "Combining linear polarization spectroscopy and the Representative Layer Theory to measure the Beer–Lambert law absorbance of highly scattering materials". In: *Analytica chimica acta* 853 (2015), pp. 486–494 (cit. on p. 29).

[104] Suibin Luo, Shuhui Yu, Rong Sun, and Ching-Ping Wong. "Nano Ag-deposited BaTiO3 hybrid particles as fillers for polymeric dielectric composites: toward high dielectric constant and suppressed loss". In: *ACS applied materials & interfaces* 6.1 (2013), pp. 176–182 (cit. on p. 33).

[105] Jiongxin Lu, Kyoung-Sik Moon, Jianwen Xu, and CP Wong. "Synthesis and dielectric properties of novel high-K polymer composites containing in-situ formed silver nanoparticles for embedded capacitor applications". In: *Journal of Materials Chemistry* 16.16 (2006), pp. 1543–1548 (cit. on p. 37).

[106] M Hikita, M Nagao, G Sawa, and M Ieda. "Dielectric breakdown and electrical conduction of poly (vinylidene-fluoride) in high temperature region". In: *Journal of Physics D: Applied Physics* 13.4 (1980), p. 661 (cit. on p. 39).

[107] Douglas R Dillon, Kishore K Tenneti, Christopher Y Li, Frank K Ko, Igors Sics, and Benjamin S Hsiao. "On the structure and morphology of polyvinylidene fluoride–nanoclay nanocomposites". In: *Polymer* 47.5 (2006), pp. 1678–1688 (cit. on pp. 42, 43).

[108] Maja Remškar, Ivan Iskra, Janez Jelenc, Srečo Davor Škapin, Bojana Višić, Ana Varlec, and Andrej Kržan. "A novel structure of polyvinylidene fluoride (PVDF) stabilized by MoS 2 nanotubes". In: *Soft matter* 9.36 (2013), pp. 8647–8653 (cit. on pp. 42, 43).

[109] Anju Toor, Hongyun So, and Albert P Pisano. "Improved Dielectric Properties of Polyvinylidene Fluoride Nanocomposite Embedded with Poly (vinylpyrrolidone)-Coated Gold Nanoparticles". In: *ACS applied materials & interfaces* 9.7 (2017), pp. 6369–6375 (cit. on p. 45).

[110] Anju Toor and Albert P Pisano. "Gold nanoparticle/PVDF polymer composite with improved particle dispersion". In: *Nanotechnology (IEEE-NANO), 2015 IEEE 15th International Conference on*. IEEE. 2015, pp. 706–709 (cit. on p. 45).

[111] Koichi Suematsu, Masashi Arimura, Naoyuki Uchiyama, Shingo Saita, and Teruhisa Makino. "High-performance dielectric thin film nanocomposites of barium titanate and cyanoethyl pullulan: controlling the barium titanate nanoparticle size using a sol–gel method". In: *RSC Advances* 6.25 (2016), pp. 20807–20813 (cit. on p. 51).

[112] Yu Song, Yang Shen, Haiyang Liu, Yuanhua Lin, Ming Li, and Ce-Wen Nan. "Enhanced dielectric and ferroelectric properties induced by dopamine-modified BaTiO 3 nanofibers in flexible poly (vinylidene fluoride-trifluoroethylene) nanocomposites". In: *Journal of Materials Chemistry* 22.16 (2012), pp. 8063–8068 (cit. on p. 51).